RADC-TDR-63-237

FINAL REPORT

SUBMILLIMETER-WAVE COMPONENT DEVELOPMENT

TECHNICAL DOCUMENTARY REPORT NO. RADC-TDR-63-237

May 1963

Rome Air Development Center
Research and Technology Division
Air Force Systems Command
United States Air Force
Griffiss Air Force Base, New York

Project No. 5578, Task No. 55284

(Prepared under Contract AF 30(602)-2758 by J. J. Taub and H. J. Hindin of Airborne Instruments Laboratory, a Division of Cutler-Hammer, Inc., Deer Park, Long Island, New York.)

RADC-TDR-63-237

FINAL REPORT

SUBMILLIMETER-WAVE COMPONENT DEVELOPMENT

TECHNICAL DOCUMENTARY REPORT NO. RADC-TDR-63-237

May 1963

Rome Air Development Center
Research and Technology Division
Air Force Systems Command
United States Air Force
Griffiss Air Force Base, New York

Project No. 5578, Task No. 55284

(Prepared under Contract AF 30(602)-2758 by J. J. Taub and H. J. Hindin of Airborne Instruments Laboratory, a Division of Cutler-Hammer, Inc., Deer Park, Long Island, New York.)

NOTICE

When Government drawings, specifications, or other data are used for any purpose other than in connection with a definitely related Government procurement operation, the United States Government thereby incurs no responsibility nor any obligation whatsoever; and the fact that the Government may have formulated, furnished, or in any way supplied the said drawings, specifications, or other data, is not to be regarded by implication or otherwise as in any manner licensing the holder or any other person or corporation, or conveying any rights or permission to manufacture, use, or sell any patented invention that may in any way be related thereto.

FOREWORD

This report was prepared by Airborne Instruments Laboratory, a Division of Cutler-Hammer, Inc., Deer Park, Long Island, New York on Air Force Contract AF 30(602)-2758, under Task No. 55284 of Project No. 5578, "Submillimeter-Wave Component Development." The work was administered under the direction of the Research and Technology Division. Messrs P. Romanelli and J. LoMascolo were Section Chief and Project Engineer, respectively.

The studies presented began in July 1962, were concluded in March 1963, and represent the work of the Department of Applied Electronics of Airborne Instruments Laboratory. J. J. Taub was project director.

The cooperation of B. F. Thaxter, P. Tannenwald, and G. S. Heller of the Lincoln Laboratory at the Massachusetts Institute of Technology is gratefully acknowledged for permitting us to use their carcinotron.

This report is the final report and concludes the work on Contract AF 30(602)-2758. The contractor's report number is 2098-1.

A paper, "Submillimeter Components Using Oversize Quasi-Optical Waveguide," by J. J. Taub, O. F. Hinckelmann, H. J. Hindin, and M. L. Wright was presented at the IEEE Professional Technical Group on Microwave Theory and Techniques Conference on Millimeter and Submillimeter Waves held at Orlando, Florida in January 1963. The paper has been accepted for publication in the September 1963 Transactions on Microwave Theory and Techniques.

A technical note, entitled "Permittivity Measurements at Submillimeter Wavelengths," by J. J. Taub and H. J. Hindin has been accepted for publication in The Review of Scientific Instruments.

ABSTRACT

Techniques for the design, construction, and evaluation of a 10-db directional coupler, a 0 to 40 db variable attenuator, a 90-degree phase shifter, and a duplexer to operate in the 300 to 1000 Gc region were investigated theoretically and experimentally. Quasi-optical, oversize, trough, and Goubau-beam waveguide were studied. Quasi-optical techniques used in oversize waveguide were found to be most suitable and were used in constructing the components. These components were evaluated at 0.9-mm wavelength. The experimental data showed good agreement with the design theory. Thus, submillimeter components using quasi-optical techniques in oversize waveguide can be successfully designed and fabricated. Some components had higher insertion loss than desired due to the dielectric dissipation effects. These losses are reduced by using a multiple-dielectric-slab coupling structure.

TABLE OF CONTENTS

LIST OF ILLUSTRATIONS

I. INTRODUCTION

Contract AF 30(602)-2758 requires the design and fabrication of components that can operate in the 300 to 1000 Gc range (submillimeter wavelengths). The following waveguide techniques were evaluated from the point of view of electrical performance and ease of construction:

1. Trough,
2. Goubau-beam,
3. Quasi-optical,
4. Oversize.

The use of these techniques in the following components was evaluated:

1. Directional coupler--10-db coupling with 30-db directivity,
2. Variable attenuator--0 to 40 db attenuation,
3. Phase shifter--90 degree or greater phase shift,
4. Duplexer--20-db transmitter-to-receiver isolation.

The effort consisted of:

1. Determining the most suitable technique for component development,
2. Designing and fabricating the components,
3. Testing the components,
4. Modifying the materials and structures in accordance with the test results.

II. TECHNIQUES

At frequencies greater than 300 Gc, the use of current transmission-line and waveguide techniques is not acceptable. For example, single-mode (standard size) rectangular waveguide has a high attenuation (6 db per foot at 300 Gc) and presents construction difficulties. For dielectric surface-wave transmission lines operating at frequencies greater than 100 Gc, it becomes difficult to contain the field in a region near the dielectric, particularly when a bend is required. The overall dielectric and radiation losses are excessive, and other techniques must be investigated.

A. OVERSIZE WAVEGUIDE AND QUASI-OPTICS

Microwave radiation can generally be propagated in free space; the limiting factors are diffraction and scattering. In free space, optical principles apply if the difference in wavelength between microwave and optical frequencies is taken into account. If optical principles are suitably applied, they can be used in designing microwave components. Garnham (reference 1) has shown that these devices can be improved by enclosing them in oversize waveguide, thereby reducing losses caused by diffraction. Furthermore, these devices can be easily transported, are immune to environmental conditions (including RFI), and are relatively simple to fabricate.

Propagation in oversize waveguide approximates free-space plane-wave propagation. This can be seen from the following equation for the wavelength (λ_g) of propagation in a waveguide; that is,

$$\lambda_g = \frac{\lambda}{\sqrt{1 - (\lambda/\lambda_c)^2}}$$

where

λ = free-space wavelength corresponding to the input frequency,

λ_c = cutoff wavelength of the guide.

For 1-mm propagation in an RG-96/U K_a-band guide (10-times oversize) with a cutoff frequency of 21.1 Gc or 1.42 cm, λ_g is approximately equal to λ. Therefore, propagation in an oversize waveguide behaves like "loosely bound" free-space propagation. That is, since transmission in free space can be considered as transmission in a waveguide with infinite a and b dimensions, oversize waveguide is an approximation of these conditions. Oversize waveguide propagation can be made to occur in the TE_{10} mode with a small magnetic-field component (H_z) along the direction of propagation. Operating in this mode, it combines the advantages of propagation in standard-size waveguide and free space. Besides freedom from free-space-propagation diffraction losses, the attenuation per unit length of line is low. Figures 1 and 2 show that the losses with oversize waveguide are lower than with standard-size waveguide and free-space propagation. All components that are used in free-space propagation can be enclosed in oversize waveguide, thereby improving their operation.

The application of quasi-optical techniques in oversize waveguide has a potential multimode-propagation problem. Quasi-optical elements in these waveguides must be developed on the basis of plane reflecting boundaries to minimize mode conversion. Thus, structures such as prisms, slabs, and gratings must be used. Therefore, quasi-optics and oversize waveguide must be considered as a single technique.

In conventional waveguide propagation, the wavefront is not planar because energy reflects off the waveguide walls. A plane wave can be achieved if the waveguide is oversize enough to permit the waveguide wavelength to equal the free-space wavelength. If this plane wave is propagated (mainly in the TE_{10} dominant mode), the Poynting vector, which determines the energy propagation, is directed down the length of the waveguide in a straight line with most of the energy concentrating in the vicinity of the center of the waveguide. As a consequence, many well-known (references 2 and 3) optical elements can be adapted to operate at lower (microwave) frequencies. The basic configurations use prisms, slabs, and gratings.

One of the major problems in using oversize waveguide as a propagation medium is the presence of modes other than the dominant TE_{10}. These other modes will not generate spontaneously in the oversize waveguide because of the increased a and b dimensions, but, if they are generated by some unfavorable discontinuity, they will propagate easily. In standard waveguide, higher modes can be generated, but they decay a short distance from the discontinuity. By using a structure such as a conventional filter-coupling iris, many unwanted propagating higher modes in the oversize waveguide would propagate. Only the planar type of discontinuity can be used.

Higher modes are also propagated in the oversize waveguide by tapers that are used to connect the oversize components to the standard-size generation and detection equipment. In recent years, much work has been done in analyzing and designing mode-conversion-free tapers (reference 4). Some types of tapers that have been examined are linear, cosine, and circular arc. In general, if sufficient length is available between the cross sections to be connected by the taper (we used oversize waveguide with a b/a ratio of 1/2), mode conversion can be limited to a predetermined low level by making the taper rate of change as a function of distance in the direction of propagation approach zero. An infinitely long taper would have zero mode conversion. When the types of cross sections to be connected are not radically different in size, they can be connected with lower mode conversion (for a given length).

In conjunction with a program on multimode power measurements (reference 5), Airborne Instruments Laboratory (AIL) investigated the use of circular-arc tapers. Since large changes in cross section had to be connected within a short distance, it was found that a circular-arc taper has lower losses than a linear taper. The taper rate at each end was made to approach zero. In our initial experiments with an oversize-waveguide quasi-optical directional coupler at 3 Gc, the loss caused by mode conversion using a circular-arc taper was only a fraction of a db (reference 6).

In testing a 27-Gc coupler using quasi-optics in oversize waveguide, a different type of taper was used. It was necessary to construct a taper between S-band waveguide, which was used in the 26 to 40 Gc range and S-band waveguide, which was 10-times oversize. The length of the taper was not considered critically short, but weight and size were practical considerations. Attempts to use the same design procedure that had worked so well at 3 Gc were halted by severe mechanical problems. A curved taper of the type shown in Figure 3 would require radii so large that the taper would be essentially (for construction purposes) linear. In addition, such a device would be costly and difficult to align.

As an alternative, a 3-foot-long linear taper was used that had a discontinuous taper angle of less than 2 degrees at each end. A study of the available data indicates that, with careful manufacturing, such a taper will keep mode conversion at 27 Gc to within an acceptable level because of its gradual taper rate and small end discontinuity. A version of this taper at 1 mm is only a few inches in length and, for a 10-times cross-sectional change, would have a small flare angle and mode conversion.

B. TROUGH WAVEGUIDE

A review of the characteristics of trough waveguides was initially made using references 7, 8, and 9. The success of trough waveguide used at submillimeter wavelengths requires the deposition of thin dielectric films of less than 0.002 inch on the side walls, efficient launching structures, and low-loss tangent dielectrics. Furthermore, the trough-waveguide technique is not adequate for making the 90-degree bends required by most applications. In reference 8, it is suggested that the expected attenuation using a trough waveguide is comparable with an oversize waveguide at 1 mm.

Calculations of the attenuation of certain trough-waveguide modes show that low-loss use of the trough waveguide is theoretically feasible, but much development work will be necessary to fabricate the necessary thin films on the trough. Work done on trough waveguide shows the difficulty of theoretically designing trough-waveguide structures because of the radiation problem, and it has been suggested to use rectangular-waveguide components between lengths of trough waveguide (reference 10). Since no ideas for the practical construction of components using trough waveguide have been found, it was felt desirable to concentrate on more feasible techniques.

C. GOUBAU-BEAM WAVEGUIDE

The Goubau-beam waveguide is essentially an improvement of the quasi-optical waveguide. In normal beam transmission between two horns or antennas within the Fresnel zone (near field), the beam has a uniform diameter, but the amplitude and phase distributions vary as a function of distance along the direction of propagation. It has been shown (reference 11) that there is a beam whose amplitude and phase distributions are periodic along the propagation path. If suitable phase transformers (dielectric lenses) are placed at appropriate intervals, the original amplitude and phase distributions can be established and a new Fresnel zone formed. Such a technique can be used for the guided propagation of millimeter waves (references 11 and 12). The main losses in the system are:

1. Diffraction caused by the phase transformers,
2. Dielectric losses,
3. Reflection losses.

There are also launching and receiving losses.

This type of waveguide differs from the usual waveguide in that, instead of one particular mode propagating

(such as pure TE_{10} mode for standard-size waveguide) with a field pattern that is constant along the direction of propagation and a single propagation constant, there are many modes with a range of propagation constants and a field that varies along the direction of propagation. This multimode propagation technique makes component design difficult.

The phase transformers used at periodic intervals in the Goubau-beam waveguide are dielectric lenses that advance the phase of the outer portion of the beam relative to the center according to the relation

$$\phi = \frac{2\pi\rho^2}{\lambda D}$$

where

ϕ = phase advance at radius ρ (Figure 4),

D = spacing between phase transformers,

λ = propagating wavelength.

The maximum phase shift is:

$$\phi_{max} = \frac{2\pi R^2}{\lambda D}$$

where R is the radius of the phase transformer and is related to the diffraction loss (because of the finite size) of the lens. The desirable ϕ_{max} for low diffraction loss is 2π. For $\phi_{max} = 2\pi$, $R^2 = \lambda D$. For the 300 to 1000 Gc region, the bounding equations are

$$D = 10R^2 \qquad \text{and} \qquad D = 33.3R^2$$

for D and R in centimeters. To have proper operation of the phase transformers, the diameter must be large compared with the propagating wavelength. Typically,

$$2R = 20\lambda$$

That is, for 300 Gc, R must be at least 1 cm and D must equal 10 cm. At 1000 Gc, R must be at least 0.3 cm and D must equal 3 cm. Because of the difficulty in constructing the lens, R must be larger than these values. For an R of about 1 inch

(2.54 cm) at 300 Gc, D equals 0.641 meter, and at 1000 Gc, D equal 2.14 meters.

If R is reduced (smaller phase transformer), then ϕ_{max} is reduced and the diffraction loss is increased. This results in a smaller permissible phase-transformer spacing (D). However, the low-loss advantage of the Goubau-beam technique is lost. In addition, many transformers will be needed before the proper beam mode is established. This technique is not suitable for components in which size and weight are important.

The calculated diffraction loss of a phase transformer is given by Goubau (reference 12) as a function of the maximum phase shift of the transformer (Figure 5).

D. SUMMARY

The oversize waveguide and quasi-optical techniques are closely related and should be considered as a single technique. The oversize waveguide must use optical-type interior elements; the optical techniques may or may not be enclosed in waveguide. This technique was used exclusively in our development of submillimeter components. Since several problems must be solved before trough waveguide can be used for actual components, it could not be effectively used. The Goubau-beam technique is not applicable to the development of submillimeter components because its minimum size requirements are excessive. It is, however, an excellent means of transmitting submillimeter waves over long distances.

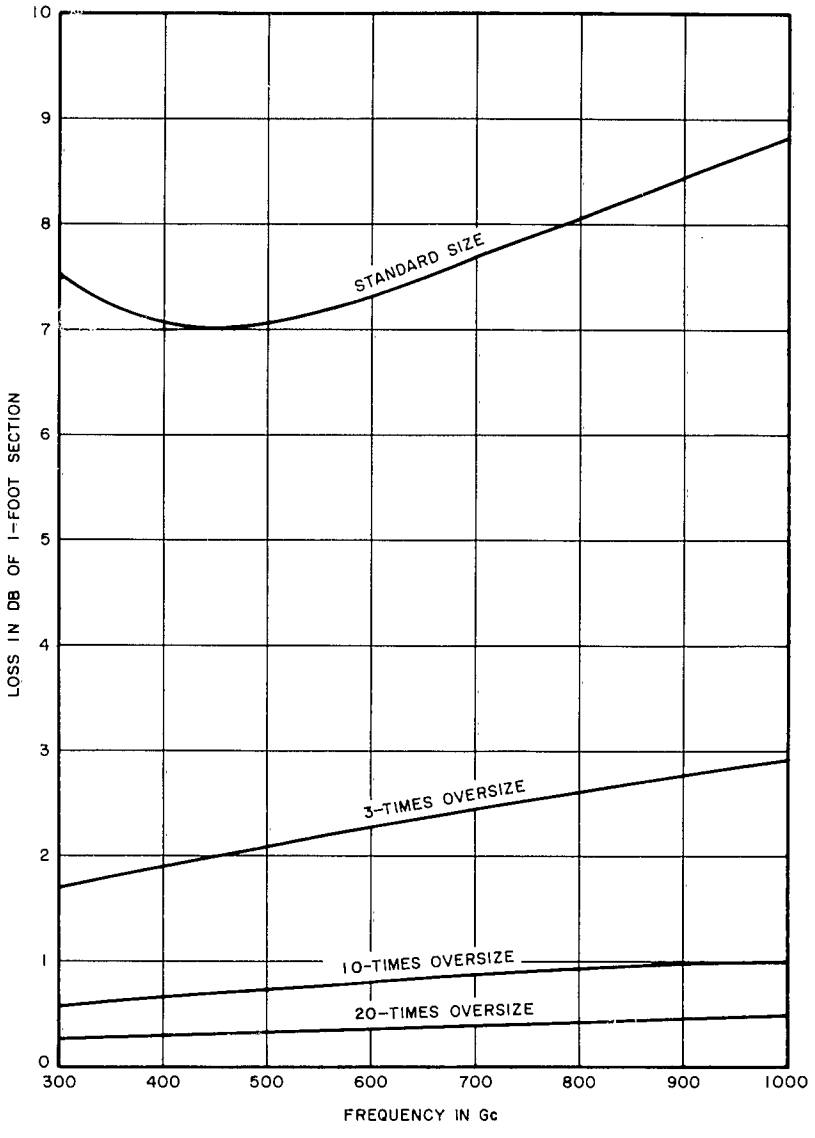

FIGURE 1. COMPARISON OF THEORETICAL LOSSES OF VARIOUS-SIZE WAVEGUIDES

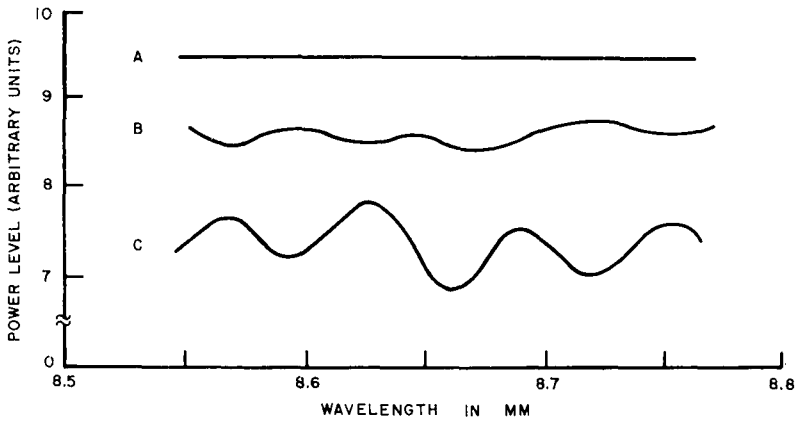

CURVE A: TRANSMISSION VIA SHORT-LENGTH WAVEGUIDE (REFERENCE LEVEL)

CURVE B: TRANSMISSION VIA HORNS WITH METAL TUBE CONNECTING THE APERTURES

CURVE C: OPTICAL TRANSMISSION BETWEEN HORN APERTURES (FREE-SPACE PROPAGATION)

DISTANCE BETWEEN APERTURES = 22.5 CM

FIGURE 2. COMPARISON OF LOSSES OF WAVEGUIDE AND FREE-SPACE TRANSMISSION LINES

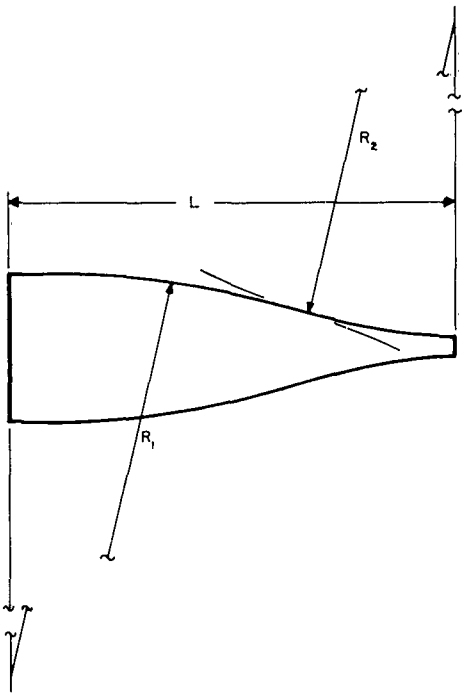

FIGURE 3. CIRCULAR-ARC TAPER FOR MINIMUM MODE CONVERSION

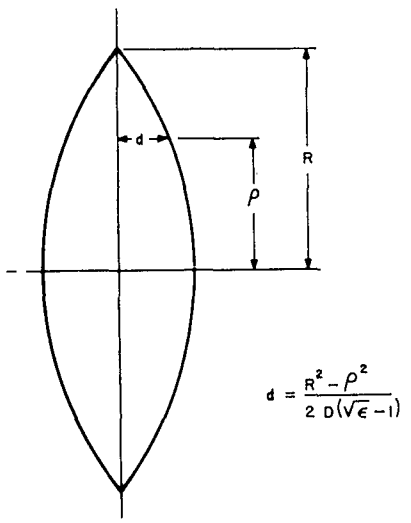

FIGURE 4. GOUBAU-BEAM PHASE-CORRECTING LENS

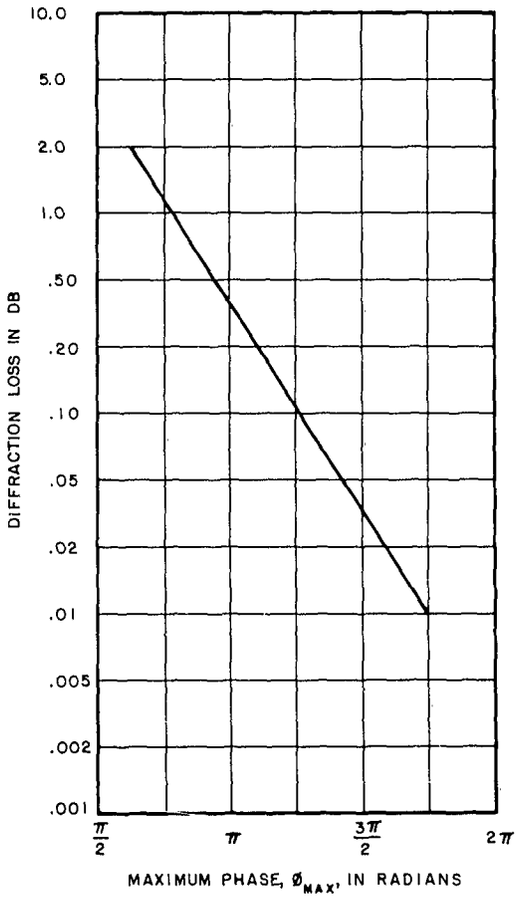

FIGURE 5. DIFFRACTION LOSS OF GOUBAU-BEAM PHASE TRANSFORMER

III. COMPONENTS

Since oversize waveguide can propagate many undesired modes, it is important to use structures that do not change the modal distribution of the incident wave. Thus, such discontinuities as screws, irises, and slits cannot be used. Optical structures such as prisms, reflectors, and gratings can be used because they operate in a uniform fashion over the entire plane wavefront. A survey of many optical devices that are useful at millimeter and submillimeter wavelengths is given in reference 3. We have designed and constructed a directional coupler, a variable attenuator, and a variable phase shifter using the double-prism beam divider described in references 3 and 13. These components were designed for operation at 0.9 mm and used 0.140- by 0.280-inch rectangular (10-times oversize) waveguide. We also constructed a circular polarization duplexer using a grating and a multiple-slab directional coupler for operation at 0.9 mm.

A. VARIABLE DIRECTIONAL COUPLER USING PRISMS

The well-known double-prism structure (reference 14) is shown in Figure 6. The effects on microwave energy passed through a double prism have been used to design components.

If a plane wave passes through an air-dielectric interface at an angle of 45 degrees, there is a dielectric constant of the material for which the phenomena of total internal reflection will occur. Consequently, the energy will undergo a 90-degree change in direction (Figure 7). The equation expressing this reflection is

$$\sqrt{\epsilon_r} \sin \theta > 1$$

where

ϵ_r = relative (to free space) dielectric constant of the material,

θ = angle of incidence of the energy on the interface.

Figure 8 shows the relationship needed between the dielectric constant and the incidence angle in order for total internal reflection to occur. Any combination of the ϵ_r and θ coordinates that gives a point in the permissible

region will result in total internal reflection. Any point in the forbidden region will not. When the two dielectric interfaces are touching (d = 0), the total internal reflection does not occur, and the energy continues in the same direction (if the reflection at the interface where the energy enters the dielectric is neglected).

For an intermediate value of d not equal to zero or infinity (one prism), it can be shown (reference 14) that total internal reflection occurs, and power (depends on d) can be coupled into the second prism to proceed in the original direction of propagation because of the evanescent (exponentially decaying) wave from the first interface. As shown in Figure 6, the energy divides into three directions. The percent that goes to ports 2 and 3 is a function of only λ, ϵ_r, and d, and no energy goes to port 4 (neglecting dielectric dissipation). There is a 90-degree phase shift between the waves going to ports 2 and 3.

The double prism is a fundamental element in the development of oversize-waveguide quasi-optical components. It behaves the same way for power introduced at any port and is the optical equivalent of the conventional microwave directional coupler with a 90-degree phase difference between ports 2 and 3. With modifications, this structure can be used to make the desired 10-db coupler, variable attenuator, and phase shifter. It can also act as a duplexer when set in the 3-db coupling position provided a 6-db additional loss in the received power can be tolerated.

In the double-prism 10-db coupler, energy can be introduced at any port, and the device will divide the power at a desired ratio with a decoupled port. By varying d, the power division can be changed with an external adjustment. A 10-db setting was used in accordance with the objectives of the contract.

If the device is considered to be lossless and reflectionless, the prism power division is completely determined. For straight-through transmission, the ratio of the power that emerges from the device to the power that enters it is

$$\frac{P_1}{P_3} = \frac{4\epsilon_r \cos^2\theta \, (\epsilon_r \sin^2\theta - 1)}{(\epsilon_r + 1 - 2\epsilon_r \sin^2\theta) \sinh^2\alpha d + 4\epsilon_r \cos^2\theta \, (\epsilon_r \sin^2\theta - 1) \cosh^2\alpha d} \qquad (1)$$

where

ϵ_r = relative dielectric constant of prism,

d = spacing between prisms,

θ = angle of incidence of energy at air-dielectric interface,

$\alpha = \frac{2\pi}{\lambda} \sqrt{\epsilon_r \sin^2 \theta - 1}$.

The straight-through attenuation (in db) is defined as

$$A = 10 \log \frac{P_1}{P_3} \qquad (2)$$

and is shown in Figure 9 as a function of d/λ for various values of ϵ_r. For 10-db coupling and $\epsilon_r = 2.45$ (the measured dielectric constant of Rexolite at 0.9 mm), the setting of d is determined from $d/\lambda = 0.5$.

Before designing a 0.9-mm device, we constructed a 10-db directional coupler using a 10-times oversize waveguide operating at about 27 Gc. Its purpose was to test the design principles. The results of the tests are shown in Figure 10. Linear tapers with a small taper rate (less than 2 degrees) were used to launch a TE_{10} mode in the 10-times oversize waveguide. The two Rexolite prisms were separated by an air space of thickness d. Quarter-wavelength dielectric slabs were used to match the prisms to the 4 waveguide ports. This coupler has a coupling that is constant to within a few tenths of a db over a 1.83-percent bandwidth with a total insertion loss of about 1 db. This was caused by losses in the tapers, dielectric prisms, and waveguide walls. The input SWR was about 1.3, showing that further matching could yield better operation. Over a 500-Mc bandwidth, the power in the decoupled arm is at least 30 db below the power in port 3, which is nearly 10 db below the input-port level.

The success of the 27-Gc coupler indicated that the quasi-optical oversize-waveguide coupler at submillimeter wavelengths could be built provided that a careful dimensional scaling was effected. Such a device was designed and constructed.

The 0.9-mm directional coupler consists of two crossed waveguides with a pair of dielectric prisms that are separated by a distance d and placed at the center of the

structure (Figure 11A). The prism surfaces must be matched to the 4 ports if it is desired to make the shapes of the experimental power-ratio curves agree with the theoretical predictions. Matched prisms were obtained by slotting the surfaces facing the 4 ports using design equations given by Garnham (reference 1). The slot size at 0.9 mm using Rexolite prisms is (Figure 11B):

$$a = 0.0022 \text{ inch}$$

$$a + b = 0.008 \text{ inch}$$

$$s = 0.0067 \text{ inch}$$

These slots were cut parallel to the direction of polarization of the electric field. Figure 12 is a photograph of a slotted Rexolite prism designed for operation at 0.9 mm. The quartz prisms were matched by using quarter-wave teflon slabs.

Figure 13 is a photograph of the directional coupler. The separation of the prisms is adjusted by a micrometer-driven wheel that is connected to one of the prisms by a Rexolite tab projecting from the prism closest to the micrometer. The other prism is stationary. The crossed waveguide is constructed from a three-sided brass waveguide with a top wall bolted into position. The surface finish on the waveguide walls is less than 5 microinches. This device can be adjusted for any desired coupling ratio by adjusting the micrometer.

Initial tests on the 0.9-mm coupler were made with unmatched Rexolite prisms. The measurements were made using the carcinotron at Lincoln Laboratories. Figures 14 and 15 show the attenuation in the straight-through and perpendicular arms. The experimental results showed such good agreement with the predicted results that a matched Rexolite directional coupler was constructed and tested. Figures 16 and 17 show the attenuation in the straight-through and perpendicular arms of the matched directional coupler. Measurements of decoupled-port power level showed a directivity greater than 20 db. Dielectric attenuation losses were high--about 6 db for the Rexolite prisms.

A directional coupler was built using a matched quartz device. The results of attenuation measurements are shown in Figure 18. The directivity was found to be greater than 20 db and a 10-db coupling was obtained by appropriate micrometer adjustment. The 10-db directional coupler was found to operate quite well at submillimeter wavelengths. The only problem was a high dielectric loss.

B. VARIABLE ATTENUATOR USING PRISMS

The basic 4-port directional coupler with a quasi-optical coupling element was modified to a 2-port attenuator.

The input SWR of this attenuator is low because it is only a function of air-dielectric interface reflections. The SWR is minimized by using matching techniques. The insertion loss is a function of both the waveguide-wall losses, which are minimal for the short length of oversize waveguide, and the dielectric losses. The dielectric loss is large because of the high loss tangent of the dielectric-prism materials. Large variations in attenuation range are theoretically possible; the 0 to 40 db specification is easily achieved.

Figure 19 shows the 0 to 40 db double-prism variable attenuator. This device was tested at 125 Gc to obtain an indication of its behavior as far as material losses and operating characteristics are concerned. Also, since the performance of the component is theoretically predictable at any frequency, it was a good test of the general usefulness of the principles involved.

At 125 Gc (obtained from the Amperex DX-237 klystron), the 10-times oversize waveguide (at 0.9 mm) used to make the variable attenuator was only 3-times oversize, and there was some minor deterioration in the behavior of this device since the propagated wavefront was not completely planar. We also expected a higher waveguide loss. The two prisms were unmatched to the 125-Gc signal. Furthermore, we did not expect to obtain a 40-db attenuation range because the attenuation is almost linear with d/λ. Thus, for a given d, an increase in λ causes a decrease in d/λ and in the available attenuation.

Figure 20 shows the attenuation versus prism separation for the variable attenuator at 125 Gc. Each 0.001 inch of travel of the prism from zero separation is equivalent to a change of about 0.2 db. Above 2 or 3 db, the attenuation becomes linear with d. This variable attenuator can be calibrated theoretically by using equation 2.

The experimental results show good agreement with the expected results. The errors that occur are due to the inability to obtain (1) a true zero prism separation and, (2) a totally planar wavefront impinging on the prisms (waveguide is only 3-times oversize). Thus, instead of a 45-degree angle of incidence on the prism interface, there is a small spectrum of angles around 45 degrees. The prisms are also mismatched causing reflections at all 4 air-dielectric interfaces.

Measurements were then made at 0.9 mm using the carcinotron at Lincoln Laboratories. The variable attenuator used was not matched at 0.9 mm. The results are shown in Figure 21 and are in close agreement with the theoretical predictions; they also provide the first accurate measurement (Section VI-A) of the dielectric constant of Rexolite at 0.9 mm ($\epsilon_r = 2.45$)

The measured loss of the unmatched directional coupler was 6 db. Mode conversion, mismatch, imperfect parallelism of the prism faces, polarization, and high loss tangent account for this high figure.

The prisms were then matched by machining slots on the input and output surfaces. Figure 16 shows the attenuation of the variable attenuator. The dynamic range available was limited. Figure 16 also shows the theoretical curve of attenuation that would result if the dielectric constant of Rexolite were 2.55 (the 30 Gc value). The 0.9-mm data indicates that ϵ_r is lowered to 2.44, which is excellent agreement with the value (2.45) obtained previously.

A comparison of the experimental curve of Figure 16 with the curve of Figure 14 shows that the small half-period (with prism separation) ripple in the linear portion of the attenuation curve, which was present in the unmatched attenuator, is no longer noticeable. The small fluctuations present are basically random in the matched attenuator.

The quarter-wave transformer-matched quartz variable attenuator was tested at 0.9 mm. The results are shown in Figure 18 and are in good agreement with the theoretical predictions for an indicated dielectric constant of $\epsilon_r = 3.95$. The attenuator appeared to have an insertion loss about 1 db larger than the Rexolite attenuator for the same prism separation. There is some ripple in the attenuation-versus-prism-separation characteristic, indicating the need for improved matching.

In summary, it can be seen that the matched quartz and Rexolite prisms function as submillimeter variable attenuators with predictable characteristics. Further study must be made to find materials with lower loss tangents at these frequencies, but this does not affect the operation or feasibility of the devices.

C. MULTIPLE-SLAB DIRECTIONAL COUPLER

The double-prism structure suffers from excessive dielectric loss at frequencies greater than 300 Gc. To overcome this disadvantage, a device that requires a smaller

volume of dielectric material has been investigated (Figure 22A). The structure consists of a pair of parallel dielectric slabs, oriented at 45 degrees in relation to the incident radiation, of thickness t, and separated by an air space d_1. This device couples power from port 1 to ports 2 and 3; no power is coupled to port 4, and port 1 is matched.

The power transmitted from port 1 to port 3 is a function of d_1. The multiple-slab structure can, therefore, be used as a variable attenuator and as a directional coupler.

The theory of this device is derived in Appendix I for lossless dielectrics. The results of Appendix I for quarter-wave-thickness slabs are:

$$\frac{P_2}{P_1} = \frac{\tan^2(0.707\theta_1)\left[\left(\frac{1}{2\epsilon_r - 1}\right)^2 - 1\right]^2}{\left(\frac{2}{2\epsilon_r - 1}\right)^2 + \tan^2(0.707\theta_1)\left[\left(\frac{1}{2\epsilon_r - 1}\right)^2 + 1\right]^2}$$

and

$$\frac{P_3}{P_1} = \frac{\left(\frac{2}{2\epsilon_r - 1}\right)^2 \sec^2(0.707\theta_1)}{\left(\frac{2}{2\epsilon_r - 1}\right)^2 + \tan^2(0.707\theta_1)\left[\left(\frac{1}{2\epsilon_r - 1}\right)^2 + 1\right]^2}$$

where

P_1 = power available at port 1,
P_2 = power delivered to port 2,
P_3 = power delivered to port 3,
ϵ_r = relative dielectric constant of the slabs,
$\theta_1 = \frac{2\pi d_1}{\lambda}$.

Figure 23 shows P_3/P_1 plotted in db as a function of wavelength and slab displacement for various dielectric constants. These curves indicate that the maximum drop in transmitted power occurs at θ_1 = 127 degrees; this is a 12-db attenuation range for quartz. Thus, this structure is limited to low

coupling ratios. In addition, it is limited in its maximum attenuation when used as a variable attenuator.

To obtain a greater range of attenuation, the multiple-slab structure shown in Figure 22B was considered. The results (Figure 24) for the 2-slab case are:

$$\frac{P_2}{P_1} = \frac{\tan^2(0.707\theta_2)\left[\left(\frac{1}{2\epsilon_r - 1}\right)^4 + 1\right]^2}{4\left(\frac{1}{2\epsilon_r - 1}\right)^4 + \tan^2(0.707\theta_2)\left[\left(\frac{1}{2\epsilon_r - 1}\right)^4 + 1\right]^2}$$

and

$$\frac{P_3}{P_1} = \frac{4\left(\frac{1}{2\epsilon_r - 1}\right)^4 \sec^2(0.707\theta_2)}{4\left(\frac{1}{2\epsilon_r - 1}\right)^4 + \tan^2(0.707\theta_2)\left[\left(\frac{1}{2\epsilon_r - 1}\right)^4 + 1\right]^2}$$

where

$$\theta_2 = \frac{2\pi d_2}{\lambda}.$$

The results for n slabs are:

$$\frac{P_2}{P_1} = \frac{\tan^2(0.707\theta_n)\left[\left(\frac{1}{2\epsilon_r - 1}\right)^{2n} - 1\right]^2}{4\left(\frac{1}{2\epsilon_r - 1}\right)^{2n} + \tan^2(0.707\theta_n)\left[\left(\frac{1}{2\epsilon_r - 1}\right)^{2n} + 1\right]^2}$$

and

$$\frac{P_3}{P_1} = \frac{4\left(\frac{1}{2\epsilon_r - 1}\right)^{2n} \sec^2(0.707\theta_n)}{4\left(\frac{1}{2\epsilon_r - 1}\right)^{2n} + \tan^2(0.707\theta_n)\left[\left(\frac{1}{2\epsilon_r - 1}\right)^{2n} + 1\right]^2}$$

where $\theta_n = \frac{2\pi d_n}{\lambda}$

For this device to be a suitable variable attenuator, n must be determined for a specific attenuation range. Noting that P_2/P_1 is minimum for $0.707\theta_n = 90$ degrees, P_3/P_1 can be reduced to:

$$\frac{P_2}{P_1} = \frac{4\left(\frac{1}{2\epsilon_r - 1}\right)^{2n}}{\left[\left(\frac{1}{2\epsilon_r - 1}\right)^{2n} + 1\right]^2}$$

Then, if

$$A = 10 \log \frac{P_1}{P_2} = 20 \log \frac{1 + \left(\frac{1}{2\epsilon_r - 1}\right)^{2n}}{2\left(\frac{1}{2\epsilon_r - 1}\right)^{n}}$$

n can be determined as

$$n \approx \frac{\frac{A}{20} + 0.3}{\log (2\epsilon_r - 1)} \text{ for } \left(\frac{1}{2\epsilon_r - 1}\right)^{2n} \ll 1 \text{ (high attenuation),}$$

An analysis of the dissipation loss in a multiple-slab coupler has been made and appears in Appendix III. The purpose of the analysis is to determine whether the insertion loss is lower than that obtainable with the double-prism structure. The analysis is valid for any number of slabs. Explicit loss formulas for n = 1, 2, and 3 (equations III-10, III-11, and III-12) are:

for n = 1,

$$L = 10 \log \left[1 + \pi\epsilon_r \tan \delta \, k^2 \left(k + \frac{1}{k}\right)\right]$$

for n = 2,

$$L = 10 \log \left\{1 + \pi\epsilon_r \tan \delta \, k^2 \left[\left(k + \frac{1}{k}\right)^3 - 2\left(k + \frac{1}{k}\right)\right]\right\}$$

for $n = 3$,

$$L = 10 \log \left\{ 1 + \pi \epsilon_r \tan \delta \, k^2 \left[\left(k + \frac{1}{k} \right)^2 - 1 \right] \left(k + \frac{1}{k} \right) \left[\left(k + \frac{1}{k} \right)^2 - 3 \right] \right\}$$

where

$$k = (2\epsilon_r - 1)^{-1/2}$$

Since quartz slabs are used, we can estimate the loss by using measured values of ϵ_r and tan δ. At 0.9 mm, $\epsilon_r = 3.9$ and tan $\delta = 0.0043$ (Section VI-A). Substituting these values in equations III-10, III-11, and III-12 gives $L_1 = 0.1$, $L_2 = 0.65$, and $L_3 = 2.8$ db. Based on these calculations, it was decided to limit the number of slabs to 2. The experimental model was designed for $n = 2$ because $n = 1$ would not give a sufficient range of attenuation variation (Figures 23 and 24).

A photograph of the complete multiple-slab device is shown in Figure 25. Because of construction problems in aligning the thin slabs and maintaining proper tolerances in the spaces between the slabs, the matched quartz slab device was constructed with 2 sets of 2 slabs each ($n = 2$). It was tested at 0.9 mm using the carcinotron, and the data obtained is shown in Figure 26. This is in good agreement with the theoretical characteristics shown in Figure 24. There was sufficient range in the slab separation to permit the attenuation characteristics to be repeated as shown. The major goal was attained. The device has only 2 db of insertion loss. Although this value is higher than the predicted value it still verifies the low-loss concept. The discrepancy is mainly due to nonperfect alignment of the slabs, which causes a leakage of power into the perpendicular arm. This accounts for about 1 db. Wall losses, loss in the quartz slabs, and the imperfect directivity of the device accounts for 0.2 or 0.3 db more.

The separation between peaks of the attenuation characteristic should be 127 degrees and is measured to be 126 degrees. This again verifies the quasi-optical design theory. The only failure in this device is the inability to obtain the theoretical maximum attenuation for a given slab separation. Further study is required to determine the cause of this discrepancy, but we believe that it is related to the higher apparent insertion loss. However, the device has been shown to be a low-loss attenuator in the submillimeter region.

The directivity of the device is also shown in Figure 24. The directivity varies between 10 and 20 db but will probably be improved when the cause of the decreased attenuation range is determined.

D. GRATING DUPLEXER

When set up for operation as a 3-db hybrid, either the double-prism or multiple-slab devices can be used as duplexers. The disadvantage of such operation is the inherent 6-db loss that is present in any hybrid-type duplexer. A more satisfactory technique is to develop a submillimeter version of a circular-polarization duplexer using gratings. This grating duplexer is similar in principle to the 30-Gc device described in reference 15 but uses oversize waveguide.

Figure 27 is a diagram of the circular-polarization grating duplexer. A vertically polarized wave is launched from a transmitter and passes through grating A. This grating has slats that are oriented in such a way that the incident wave is practically unaffected. After the wave is passed through grating B, it is circularly polarized. This circularly polarized wave travels to a target where, if the target is a sheet of reflecting material, the polarization sense is reversed in the reflected wave (counterclockwise instead of clockwise, for example). When the reflected wave returns through grating B, it becomes horizontally polarized so that, when it impinges on grating A, it is totally reflected at a 90-degree angle into the receiver.

In theory, this device has no losses and perfect directivity (transmitter-receiver isolation). In practice, however, a slight loss is incurred due to the gratings, wall losses, and dielectric losses. Also, any slight grating mismatch tends to deteriorate the directivity.

Grating A consists of closely spaced metal slats that are horizontally aligned so that the vertically polarized incident wave from the transmitter goes through with little attenuation. If the spacing between the slats is such that each pair of slats acts like a cutoff waveguide for the horizontally polarized wave returning from the target through grating B, the target echo will be reflected into the receiver.

Grating B consists of closely spaced slats that are oriented 45 degrees with respect to the vertically polarized incident wave from the transmitter. This wave can be considered to have two components--one parallel and one normal (in the same plane) to the slats. The normal component passes through the grating at the free-space velocity with no attenuation. The slats serve as a group of parallel waveguides for the parallel component, and propagation occurs through the slats at a phase velocity corresponding to the slat spacing.

Because of the difficulties in constructing the gratings with only air between the slats (due to the small sizes involved), quartz strips were used for mechanical support.

For grating B, the thickness (ℓ) of each slat must be such that there is an odd multiple of 90 degrees phase difference between the horizontal and vertical components of the wave emerging from the grating to produce the desired circular polarization. This means that

$$(\beta_v - \beta_h)\ell = \frac{n\pi}{2} \text{ for } n = 1, 3, 5, \ldots \tag{3}$$

where

β_v = phase constant of vertical component,

β_h = phase constant of horizontal component.

Thus,

$$\beta_v = \frac{2\pi}{\lambda_o} \tag{4}$$

where

$\lambda_o = \frac{30}{\sqrt{\epsilon_r} f}$ in centimeters,

f = frequency in Gc.

Because the dielectric constant (ϵ_r) of quartz at 0.9 mm was unknown at the time of the grating design, we assumed that it was reasonably close to its lower frequency (30 Gc) value. A radical change would affect the attenuation range obtainable. Also,

$$\beta_h = \frac{2\pi}{\lambda_o}\sqrt{1 - \left(\frac{\lambda_o}{2a}\right)^2} \tag{5}$$

where a is the distance between the slats.

We chose n = 1 to maximize the grating bandwidth. Therefore,

$$\ell = \frac{\pi}{2(\beta_v - \beta_h)} = \frac{\lambda_o}{4\left[1 - \sqrt{1 - \frac{\lambda_o}{2a}^2}\right]} \qquad (6)$$

We can also write

$$\beta_h = \frac{2\pi}{\lambda_g}$$

where

$$\lambda_g = \frac{\lambda_o}{\sqrt{1 - \left(\frac{\lambda_o}{2a}\right)^2}}$$

so that

$$\left(\frac{2\pi}{\lambda_o} - \frac{2\pi}{\lambda_g}\right)\ell = \frac{\pi}{2}$$

A convenient ratio is $\lambda_g/\lambda_o = 1.2$. This would establish the grating dimension at practical values and also minimize higher mode propagation. With this relation,

$$2\pi\left(\frac{1}{\lambda_o} - \frac{1}{1.2\lambda_o}\right)\ell = \frac{\pi}{2}$$

or

$$\ell = 1.5\lambda_o$$

Thus, for $\lambda_o = 0.455$ mm, $\ell = 0.0269$ inch. From equation 6, a = 0.0163 inch, which would cut off the TE_{20} mode at $\lambda = a$ or 362 Gc.

For grating A, the dimensions are not critical, but the spacing between slats is such that each pair behaves as a waveguide well below cutoff at the operating frequency for waves polarized parallel to the slats.

The gratings have been matched to free space on the oversize waveguide by inserting teflon quarter-wavelength matching transformers on both sides of both gratings. The thickness of the grating is a function of the frequency and the angle of incidence of the impinging radiation. Grating A has 0.006-inch teflon matching, and grating B has 0.007-inch teflon matching.

Rectangular waveguide has been chosen to enclose the gratings for convenience (to eliminate the need for extra tapers, etc.) and to continue component design in the same fashion as the other oversize components. However, the use of rectangular waveguide instead of square waveguide when a circularly polarized wave is used results in an effective change in the degree of circular polarization between grating B and the target. To minimize this distortion (Appendix IV), the target is butted against grating B. This does not affect the tests since we are interested in the duplexer operation and not in duplexer-to-target losses.

Figure 28 shows the gratings mounted in oversize waveguide for testing. The grating duplexer was tested at 0.9 mm. It operated properly except that, at certain frequencies, the gratings did not function correctly. Essential characteristics such as grating transmission loss, transmitter receiver isolation, etc., have been measured and, except for the unexplainable frequency dependence, the device is a practical component in the submillimeter region. The tests were made at a frequency of proper operation. With the target removed and the duplexer radiating into free space, the transmitter-receiver isolation was measured to be 28 db at 0.9 mm. This exceeds the design goal of 20 db and can probably be improved. Each grating has a 2-db transmission loss. Part of this is due to losses in the quartz strips and part is due to reflections (imperfect matching). Most of the loss is probably due to the imperfect periodicity of the gratings since their small size made them difficult to construct. If grating B were producing perfect circular polarization, then the power level at the antenna arm could be expected to be equal for both horizontal and vertical polarizations. These levels were measured using a rectangular waveguide taper to a detector. The antenna and receiver waveguides were perpendicular to measure the horizontal-polarization level. This caused some error (about 1 db) since the entire area of the waveguide opening was not covered. About 2.5 db of difference still remains between the two power levels even with this cor-

rection, and it must be concluded that the circular-polarization grating was not producing perfect circular polarization. The target-to-receiver loss with the target inserted was 0.5 db and the transmitter-to-receiver loss with the target inserted was 4 db. For this duplexer, this loss should theoretically be only 0.2 or 0.3 db (due to quartz losses, wall loss, etc.), but the device still operates better than the 6-db-loss hybrid duplexer. Further work on the grating design and matching could reduce the 4-db loss. Both the 28-db transmitter-receiver isolation and the 0.5-db target-to-receiver loss are encouraging results.

In summary, the grating-duplexer characteristics were measured and, except for minor difficulties, the device operates satisfactorily. Further refinement would enhance its practicability.

E. PHASE SHIFTER

A phase shifter that provides an incremental phase shift greater than 360 degrees has been constructed. It uses a pair of matched Rexolite prisms in a 4-port H-plane cross. The incremental shift pertains to the relationship between the input arm and decoupled arm (as if the device were operated as a directional coupler). Micrometer-driven sliding shorts are used in the two coupled arms. The prism separation is adjustable permitting an accurate setting of 3-db coupling to operate the phase shifter properly at any frequency. Figure 29 is a photograph of the phase shifter.

The incremental phase shift of a signal between ports 1 and 4 is

$$\theta' = 2\theta \tag{7}$$

where

θ' = desired phase shift,

θ = electrical length traveled by the sliding short.

For this phase shifter,

$$\theta = \beta x \tag{8}$$

where

β = imaginary part of the line propagation constant,

x = distance traveled by the sliding short.

The quantity β is given by:

$$\beta = \frac{2\pi}{\lambda} \qquad (9)$$

for lossless (oversize) waveguide. By combining equations 7, 8, and 9,

$$\theta' = \frac{4\pi}{\lambda} x$$

For a 90-degree phase shifter at 0.9 mm,

$$x = \frac{\lambda}{8} = 0.0045 \text{ inch}$$

Thus, with a standard 0.5-inch micrometer drive, it is easy to obtain a phase shift greater than 360 degrees.

The sensitivity of the phase shift to the movement of the sliding short is $\Delta\theta'/\Delta x$. At 0.9 mm,

$$\Delta\theta' = 0.35\ \Delta x$$

so that, for a micrometer reading of 0.001, $\Delta\theta' = 2.0$ degrees, which is accurate for a 360-degree phase shifter.

Any unwanted signal in the directivity port caused by a slight deviation in the 3-db coupling or imperfect directivity causes a deviation in the linear characteristic of the device. To minimize these conditions, the device is matched to improve its directivity, and the prism separation is variable to maintain 3-db coupling.

To test the phase shifter, we operated it as a Michaelson interferometer at 125 Gc, 240 Gc, and 0.9 mm. One of the sliding shorts was moved along the waveguide and the other left in a fixed position. The signal in the decoupled port was periodic having alternating maxima and minima (as in a standing wave). The distance between successive maxima or minima is $\lambda/2$. Measuring the distance between many successive maxima and averaging them improves the accuracy of the wavelength determination.

The 125-Gc signal was obtained from a klystron. The klystron frequency was calibrated against known signals. With unmatched prisms, the wavelength determination of the 125-Gc signal was accurate to 1 percent. A similar result was obtained at 240 Gc. The 240-Gc signal was obtained from a haromic generator operated as a frequency doubler.

The 0.9-mm signal was obtained from the carcinotron. The frequency of the carcinotron was determined by measuring the positions of maxima and minima through the phase shifter (interferometer). The frequency of the klystron found in this fashion was 326 Gc and the calibrated frequency was 328 Gc.

Detailed studies of individual fringes were performed to determine how close the pattern obtained from the device approximated a pure standing wave pattern and to examine the presence of higher modes or nonlinear phase shift (as evidenced by a deviation from a pure standing-wave pattern). This is shown in Figures 30 and 31. Within the sources of experimental error, Figure 31 shows good mode purity. The slight flattening effect shown in Figure 30 is probably due to some abnormality in the construction of the straight-through-arm sliding short. Since the device operates properly as an interferometer, it will also operate properly as a phase shifter.

The only problem with the phase shifter was the insertion loss of the device due to the loss tangent of the prism materials. Further study of material properties in the submillimeter region would be necessary to reduce the loss and to make the phase shifter more practical. The phase shifter provides good operation at submillimeter wavelengths and has almost linear phase shift up to and greater than 360 degrees. Further work on prism matching and insertion loss could improve the device.

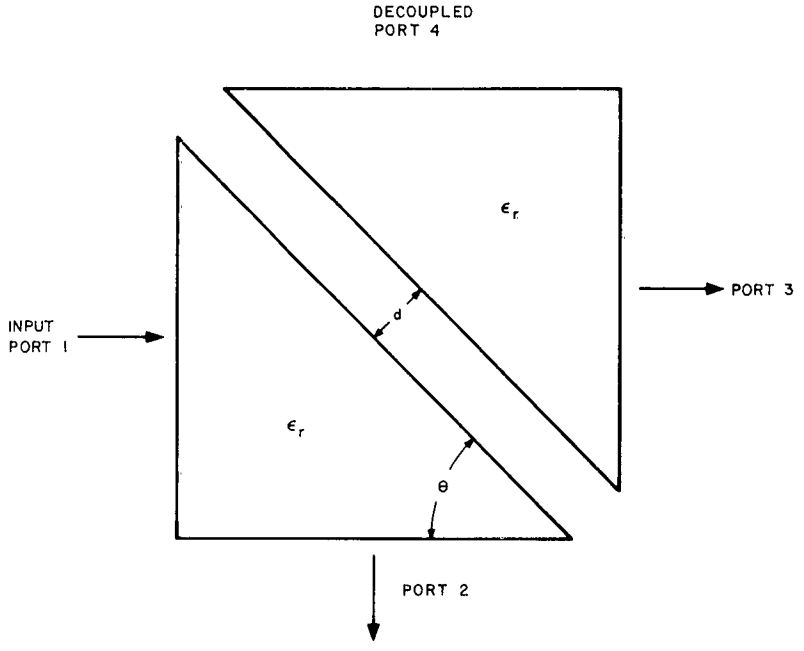

FIGURE 6. DOUBLE-PRISM STRUCTURE

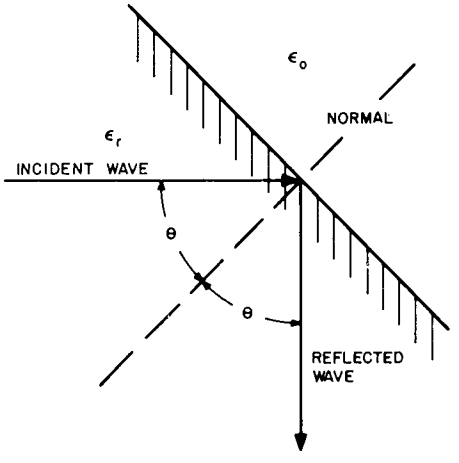

FIGURE 7. TOTAL INTERNAL REFLECTION AT 45-DEGREE INCIDENCE

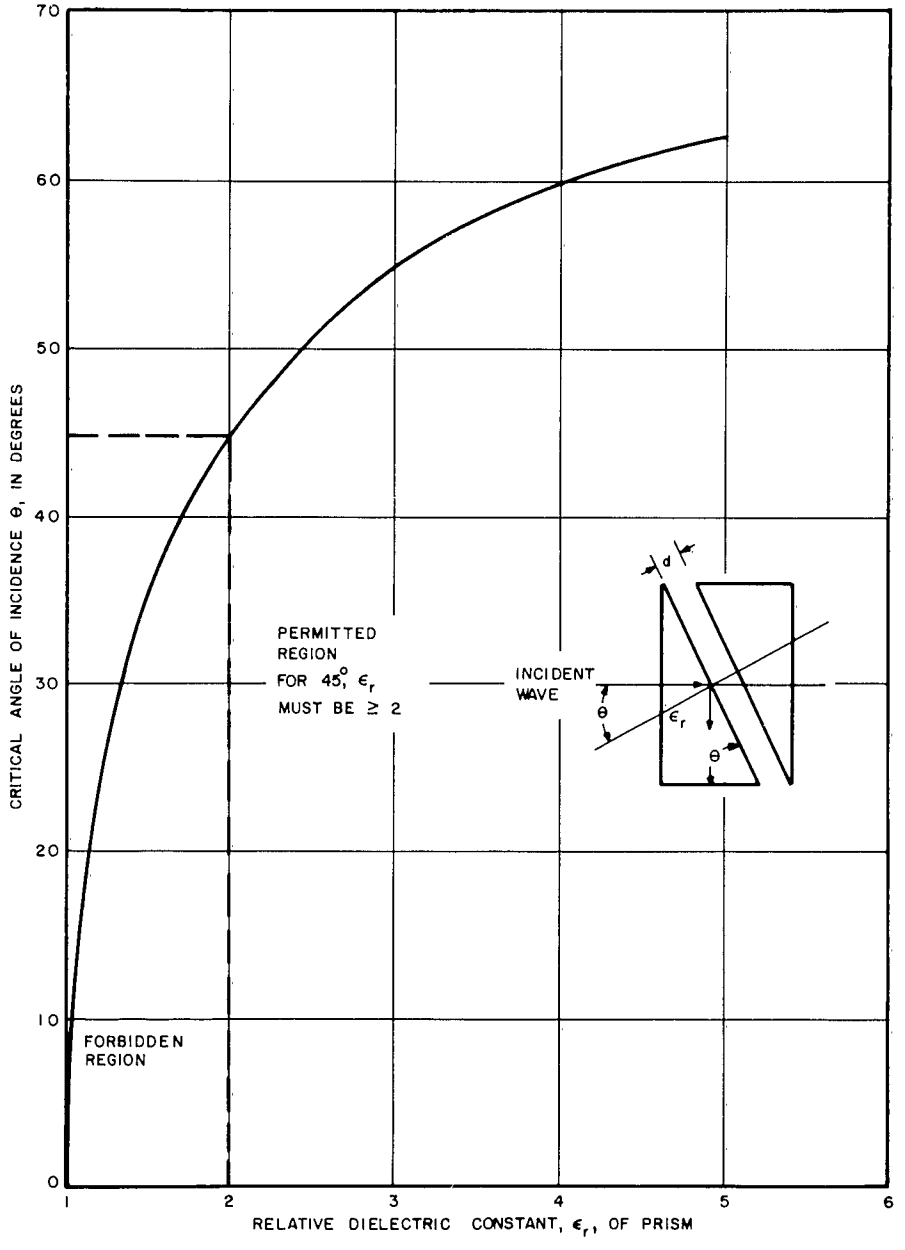

FIGURE 8. CRITICAL ANGLE OF INCIDENCE VS RELATIVE DIELECTRIC CONSTANT

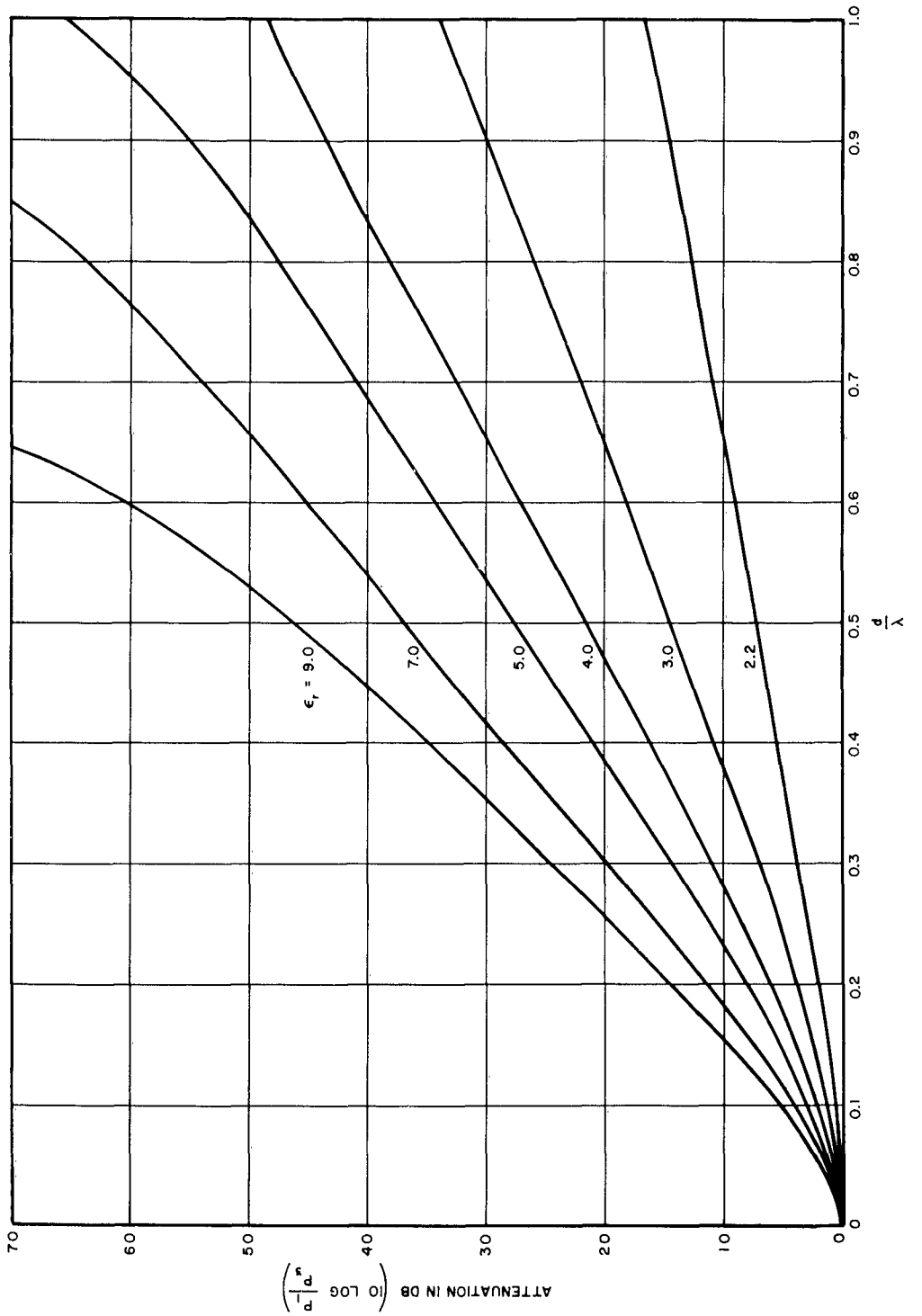

FIGURE 9. ATTENUATION OF DOUBLE-PRISM DEVICE

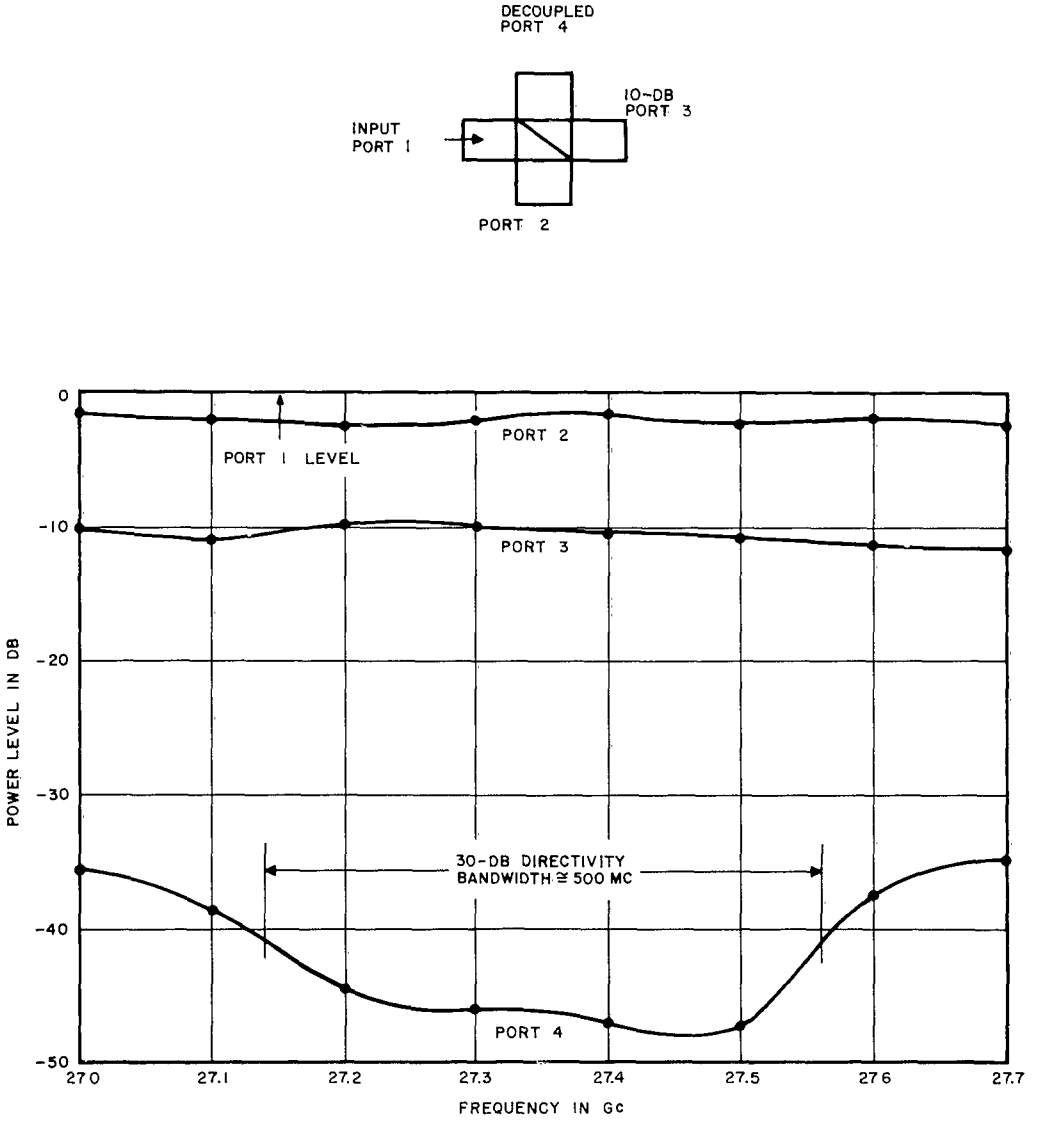

FIGURE 10. MEASURED CHARACTERISTICS OF 27-Gc DOUBLE-PRISM COUPLER

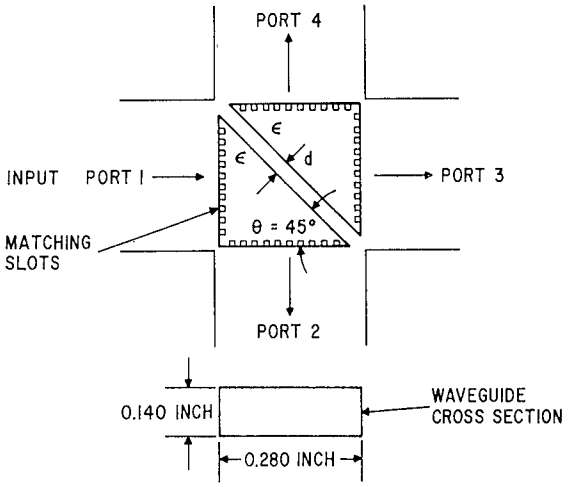

FIGURE 11. 4-PORT 300-Gc DEVICE

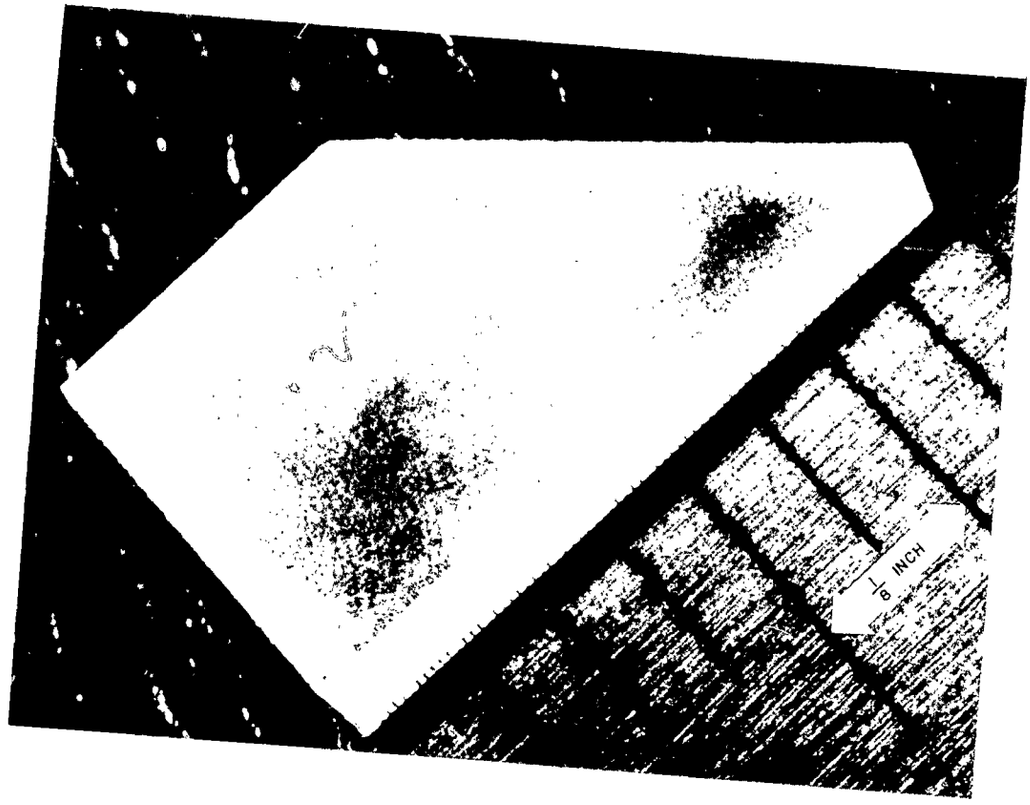

FIGURE 12. PHOTOGRAPH OF SLOTTED PRISM

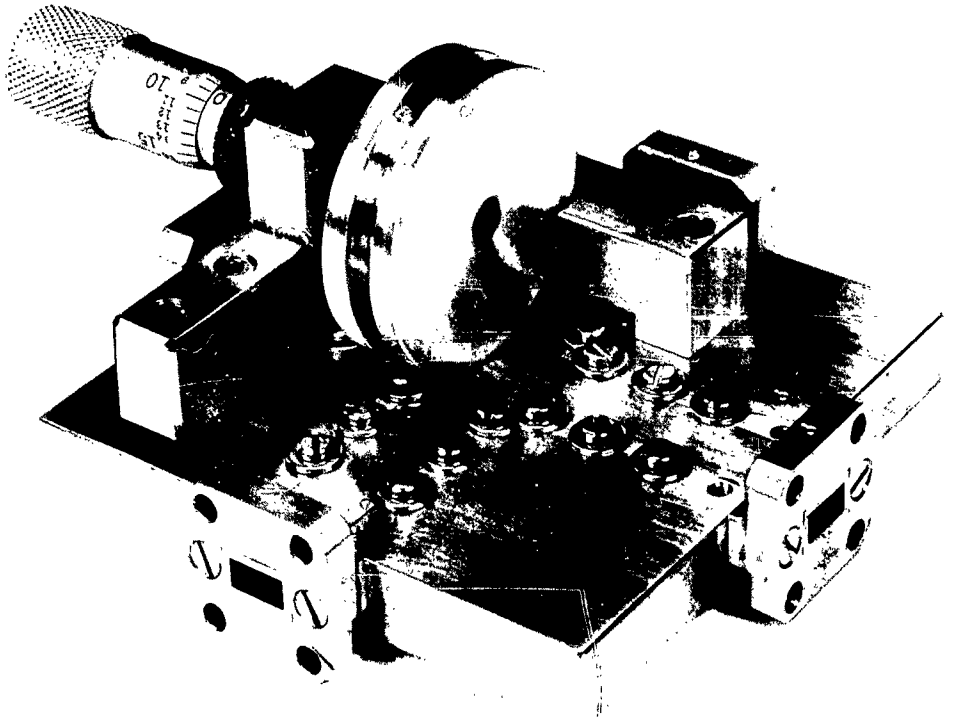

FIGURE 13. PHOTOGRAPH OF DIRECTIONAL COUPLER

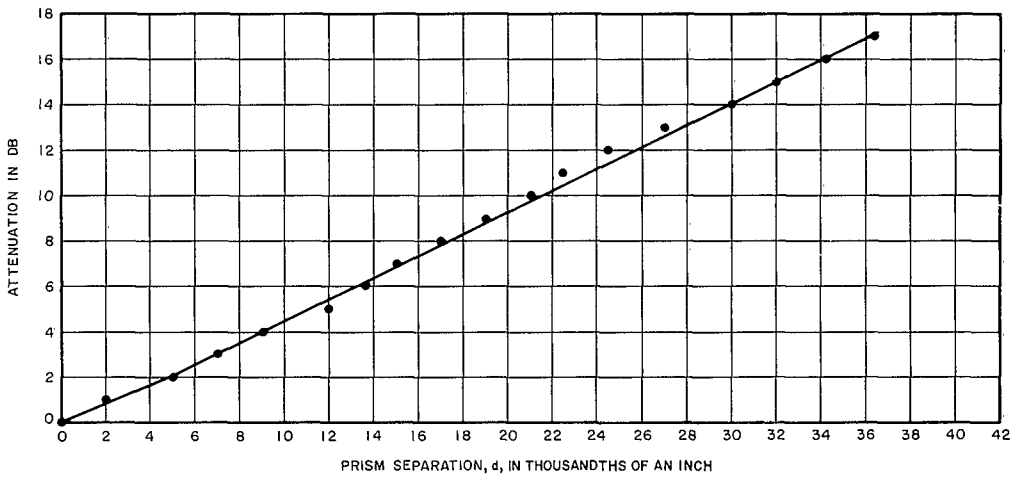

FIGURE 14. ATTENUATION IN STRAIGHT-THROUGH ARM VS PRISM SEPARATION FOR UNMATCHED REXOLITE DIRECTIONAL COUPLER AT 0.9 mm

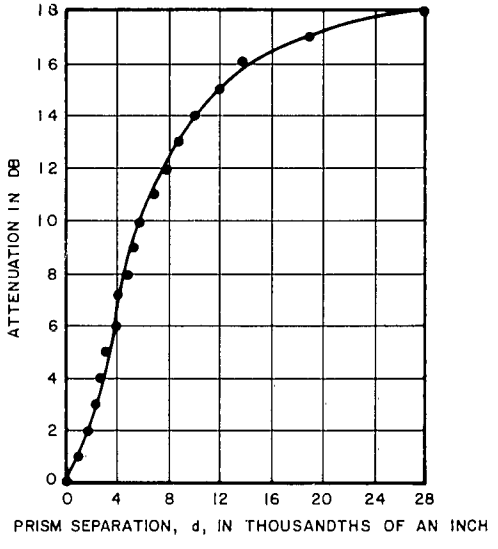

FIGURE 15. ATTENUATION IN PERPENDICULAR ARM VS PRISM SEPARATION FOR UNMATCHED REXOLITE DIRECTIONAL COUPLER AT 0.9 mm

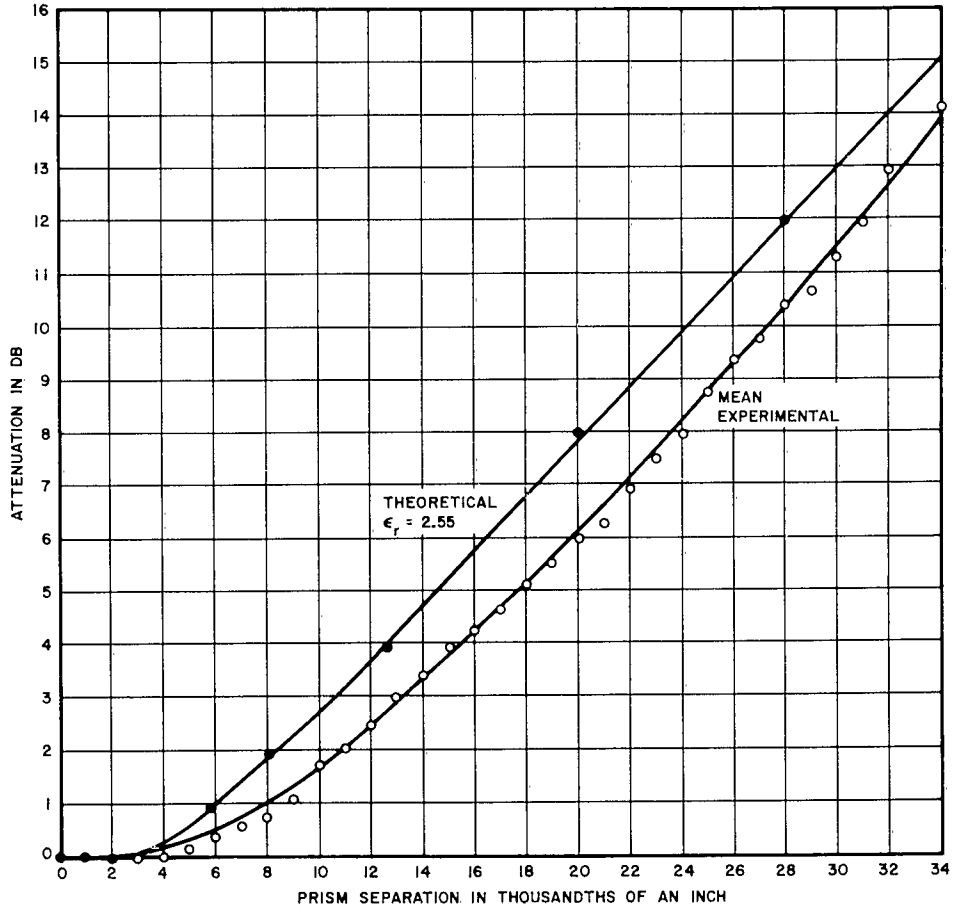

FIGURE 16. ATTENUATION IN STRAIGHT-THROUGH ARM VS PRISM SEPARATION FOR MATCHED REXOLITE DIRECTIONAL COUPLER AT 0.9 mm

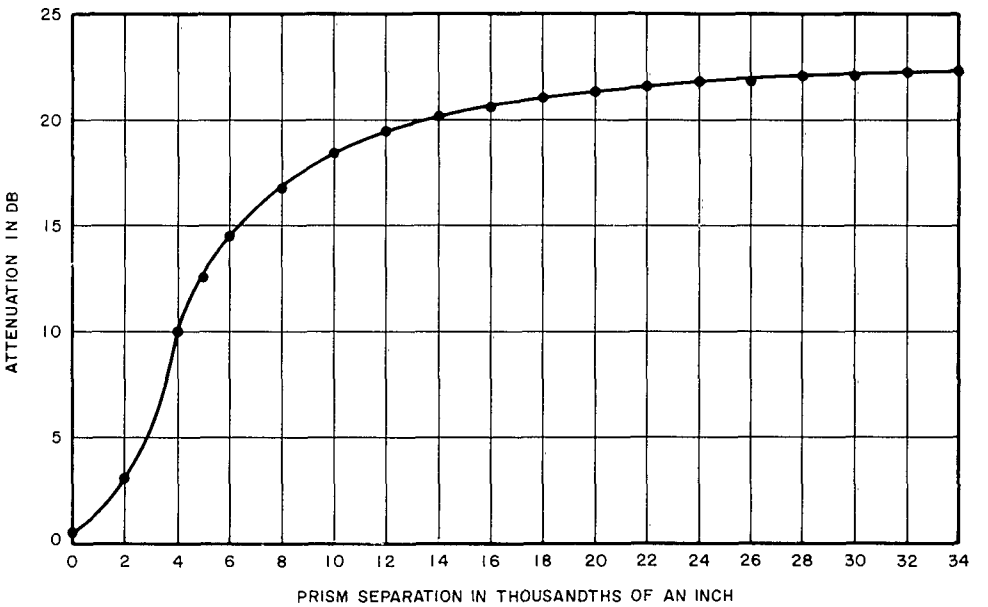

FIGURE 17. ATTENUATION IN PERPENDICULAR ARM VS PRISM SEPARATION FOR MATCHED REXOLITE DIRECTIONAL COUPLER AT 0.9 mm

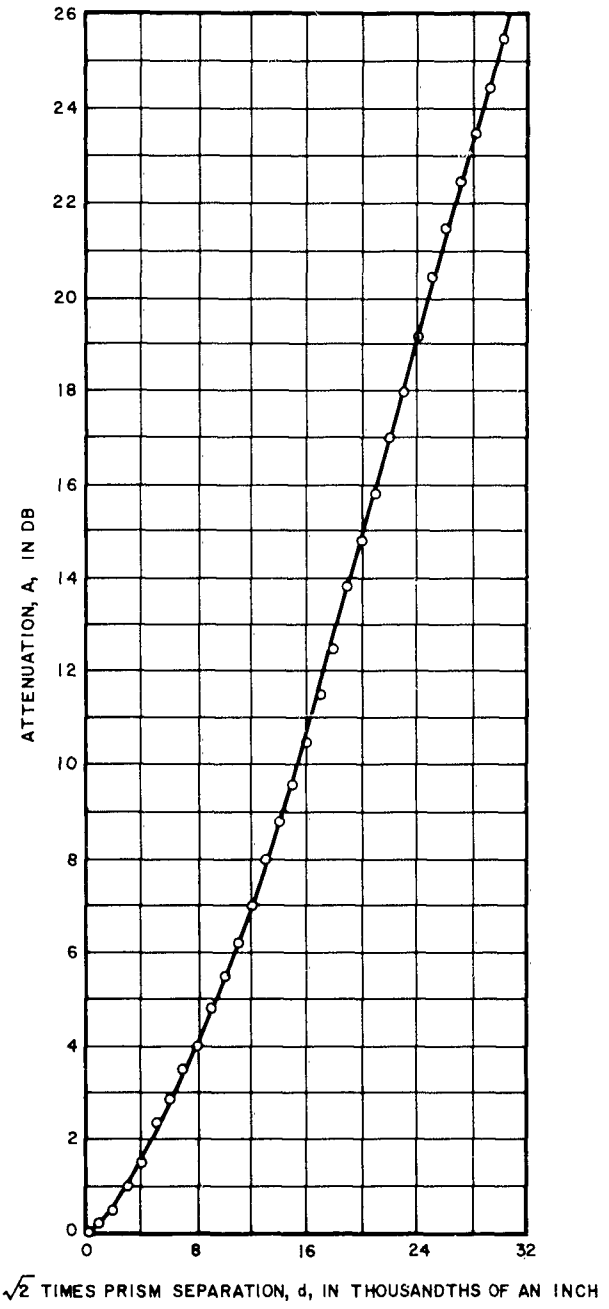

FIGURE 18. ATTENUATION STRAIGHT-THROUGH ARM VS PRISM SEPARATION FOR MATCHED QUARTZ DIRECTIONAL COUPLER AT 0.9 mm

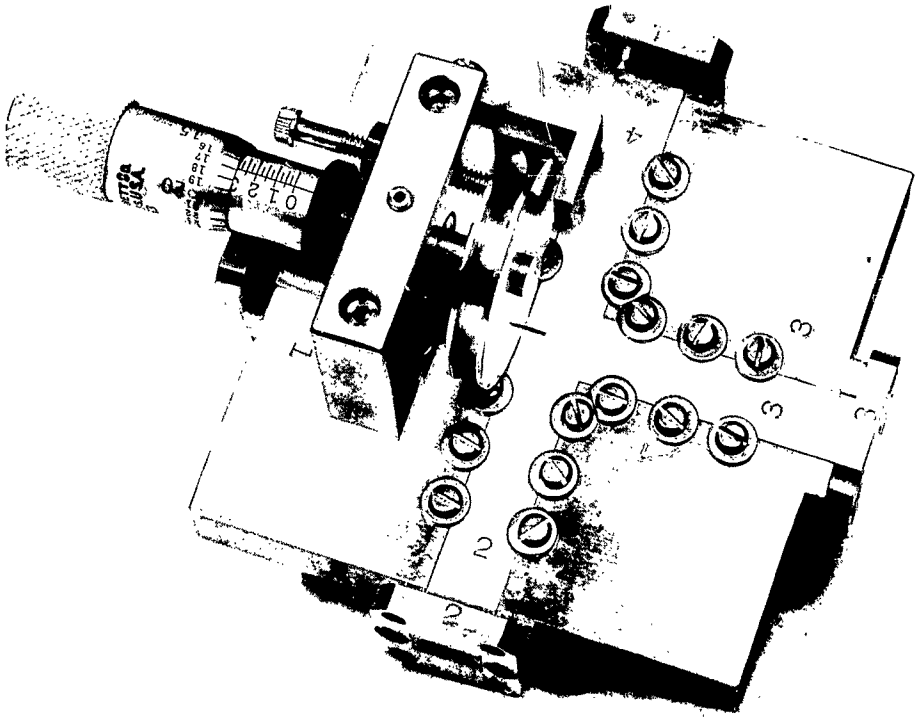

FIGURE 19. PHOTOGRAPH OF VARIABLE ATTENUATOR

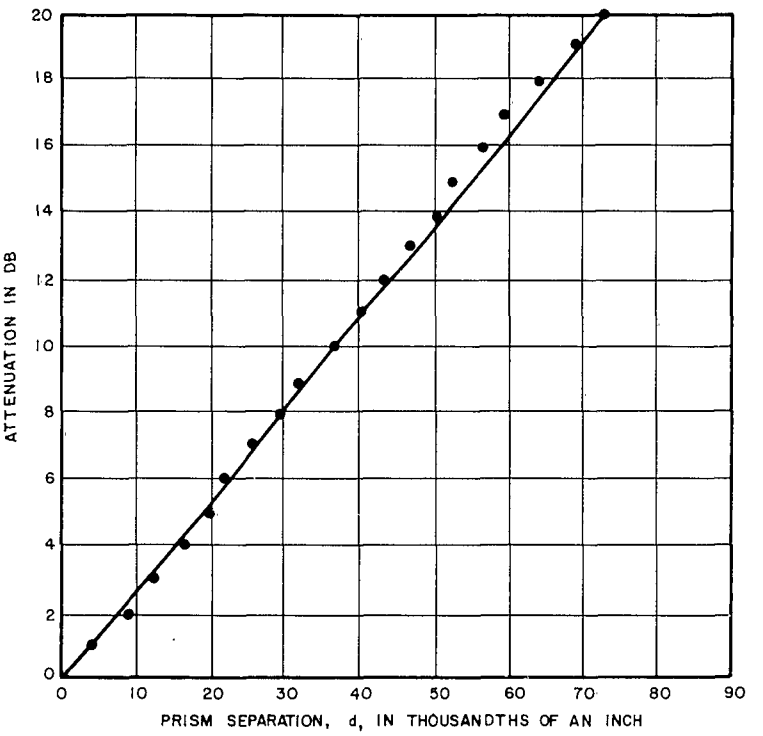

FIGURE 20. ATTENUATION IN STRAIGHT-THROUGH ARM VS PRISM SEPARATION FOR UNMATCHED 125-Gc REXOLITE VARIABLE ATTENUATOR

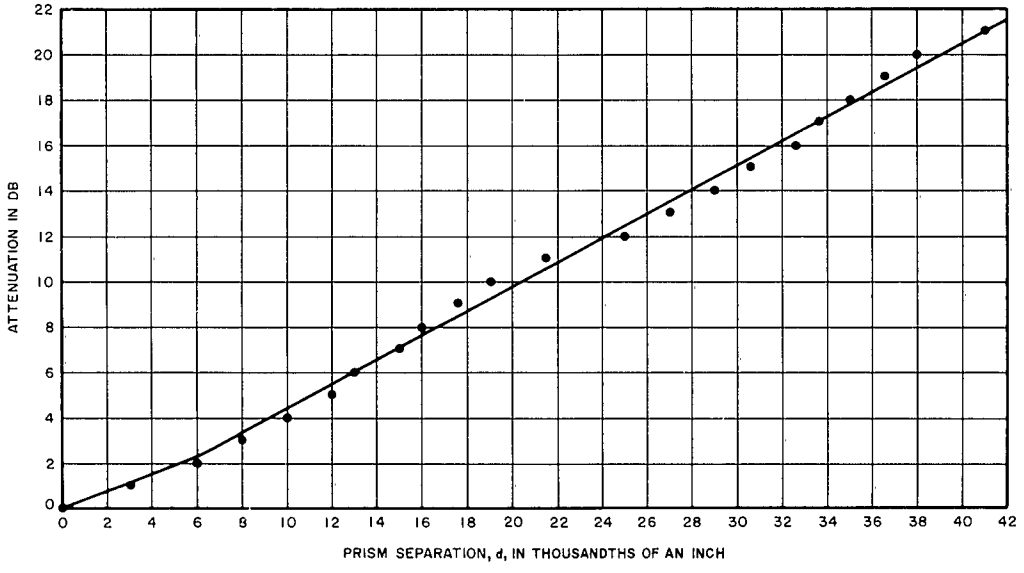

FIGURE 21. ATTENUATION IN STRAIGHT-THROUGH ARM VS PRISM SEPARATION FOR UNMATCHED 0.9-mm REXOLITE VARIABLE ATTENUATOR

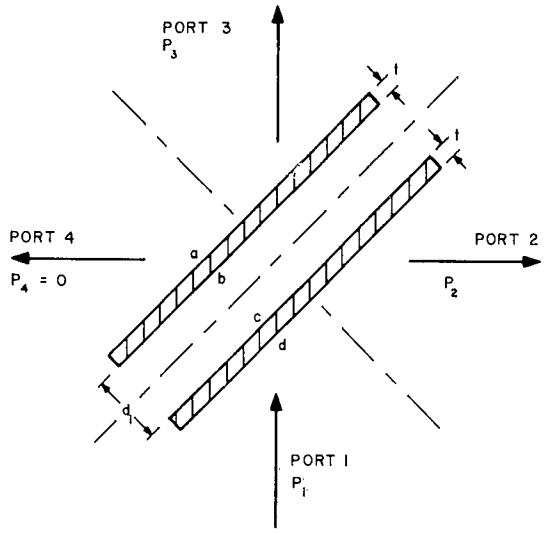

A. PAIR OF SINGLE-DIELECTRIC SLABS

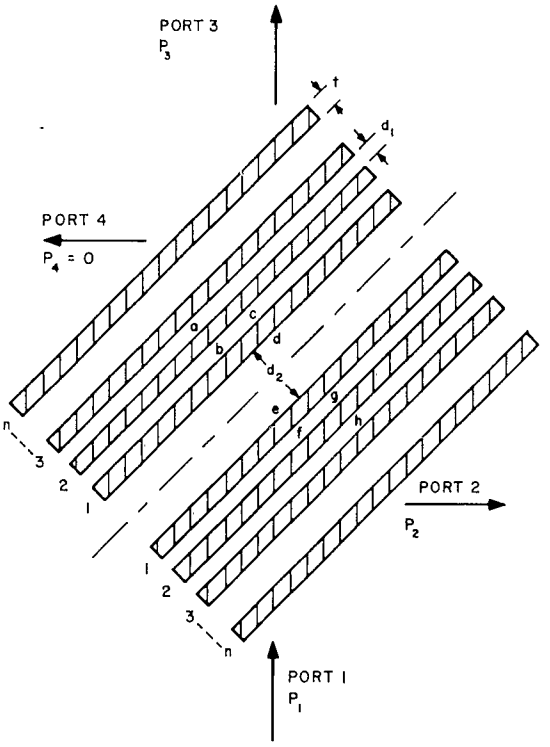

B PAIR OF MULTIPLE-DIELECTRIC SLABS

FIGURE 22. DIAGRAM OF MULTIPLE-SLAB DIRECTIONAL COUPLER

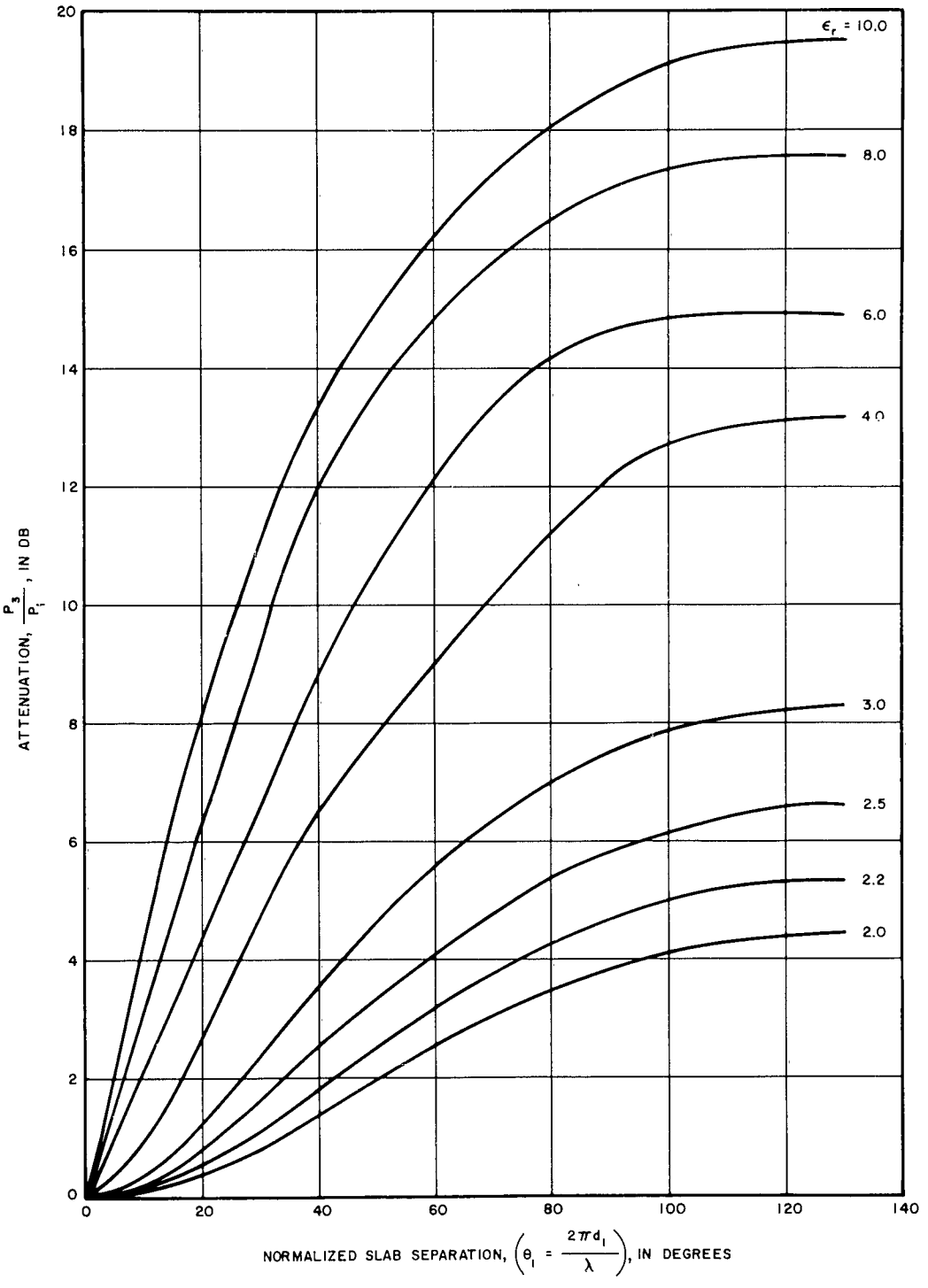

FIGURE 23. ATTENUATION IN STRAIGHT-THROUGH ARM OF n = 1 MULTIPLE-SLAB DIRECTIONAL COUPLER

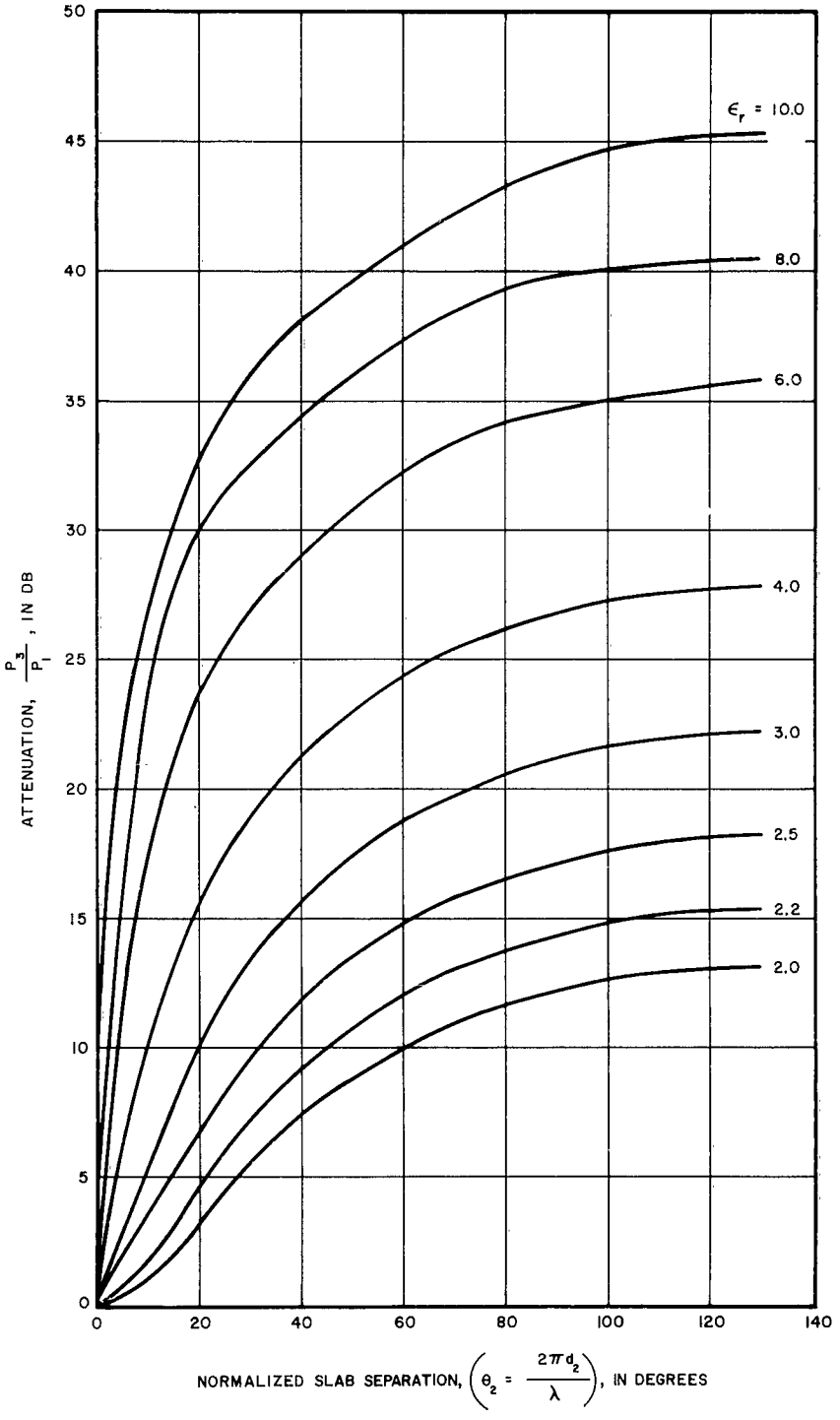

FIGURE 24. ATTENUATION IN STRAIGHT-THROUGH ARM OF n = 2 MULTIPLE-SLAB DIRECTIONAL COUPLER

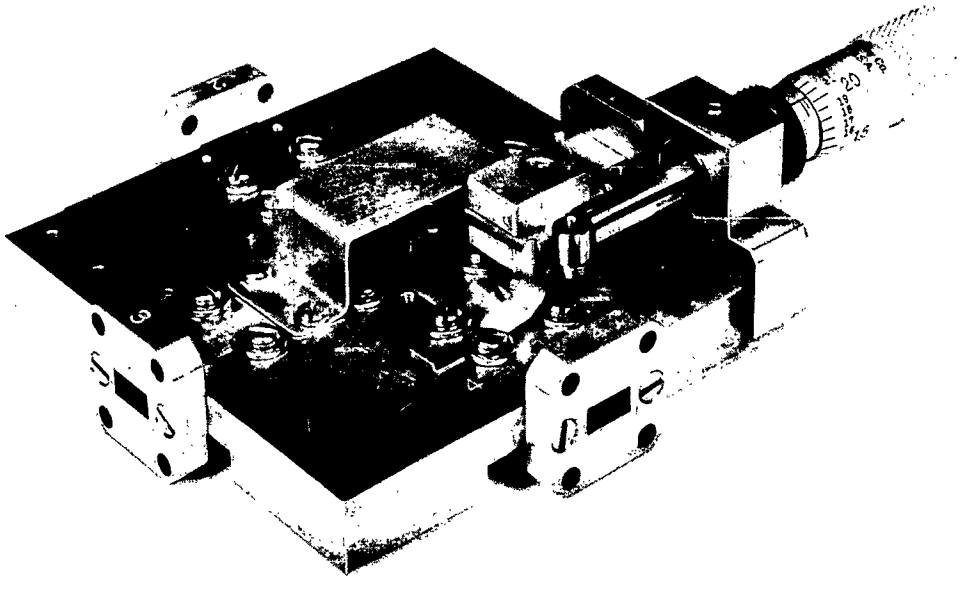

FIGURE 25. PHOTOGRAPH OF MULTIPLE-SLAB DIRECTIONAL COUPLER

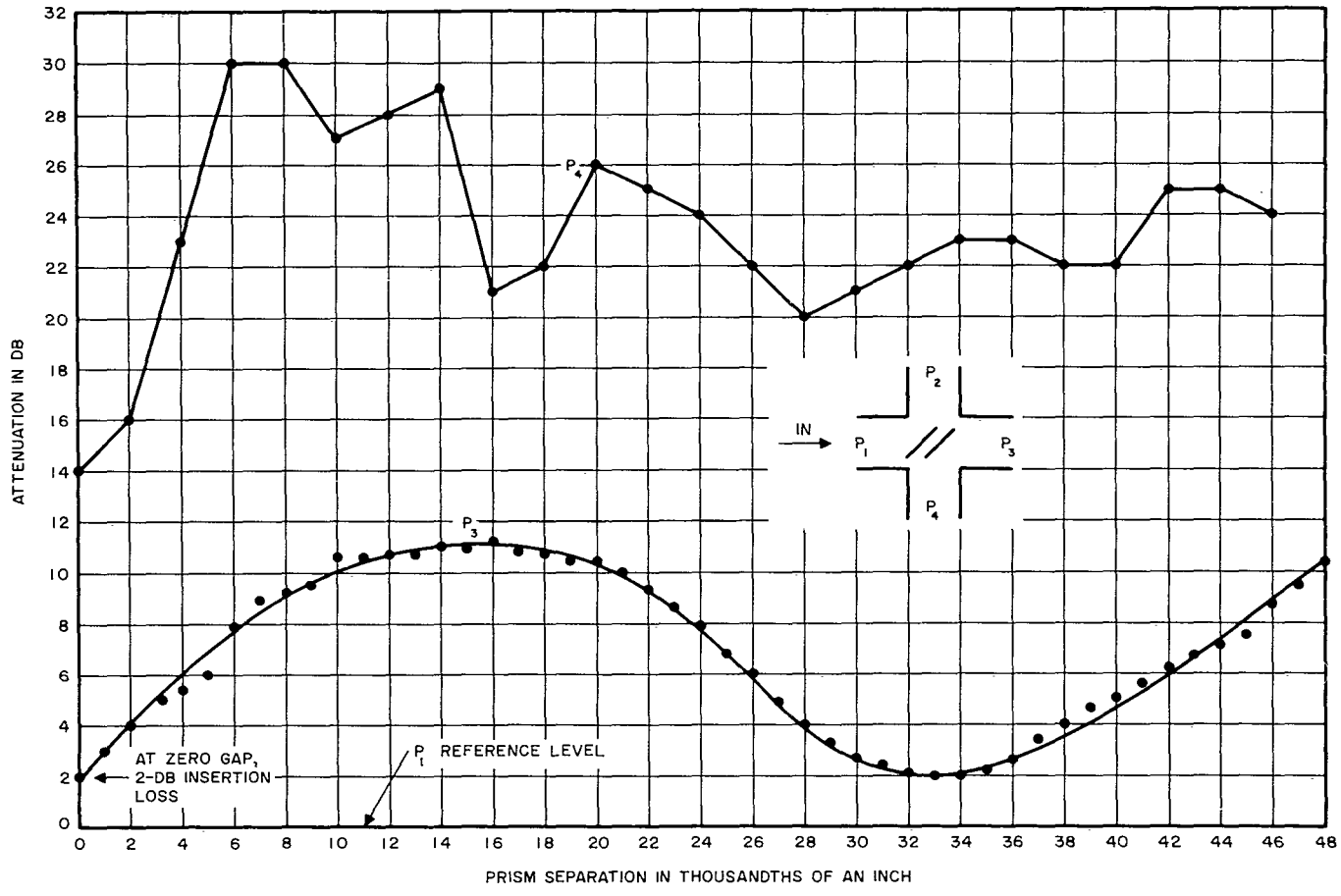

FIGURE 26. n = 2 MULTIPLE-SLAB TEST DATA

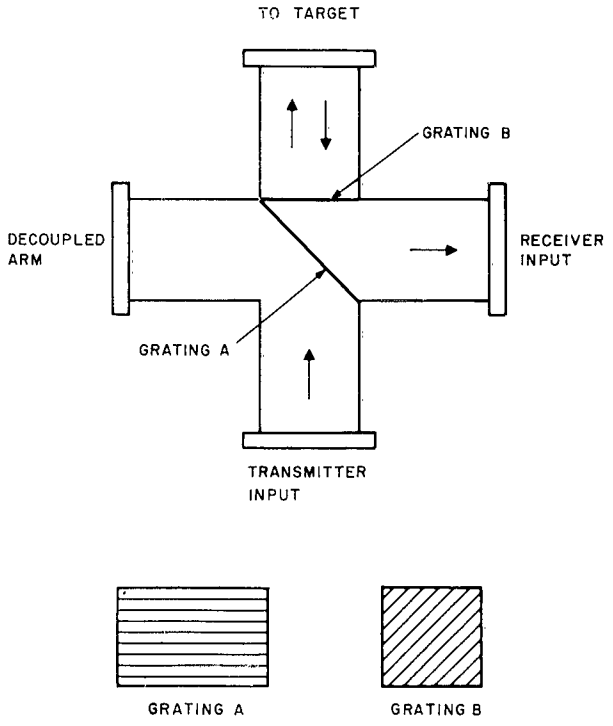

FIGURE 27. DIAGRAM OF GRATING DUPLEXER

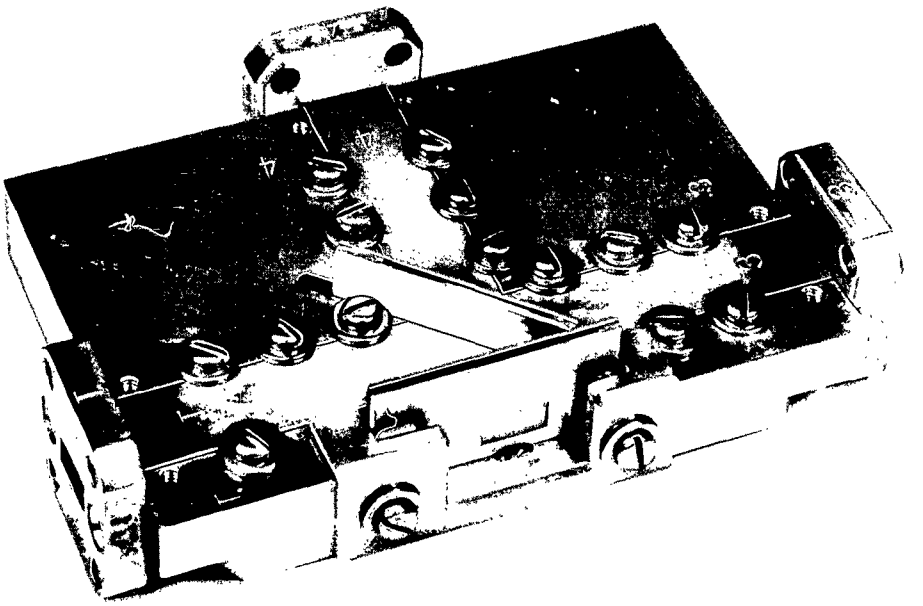

FIGURE 28. PHOTOGRAPH OF GRATING DUPLEXER

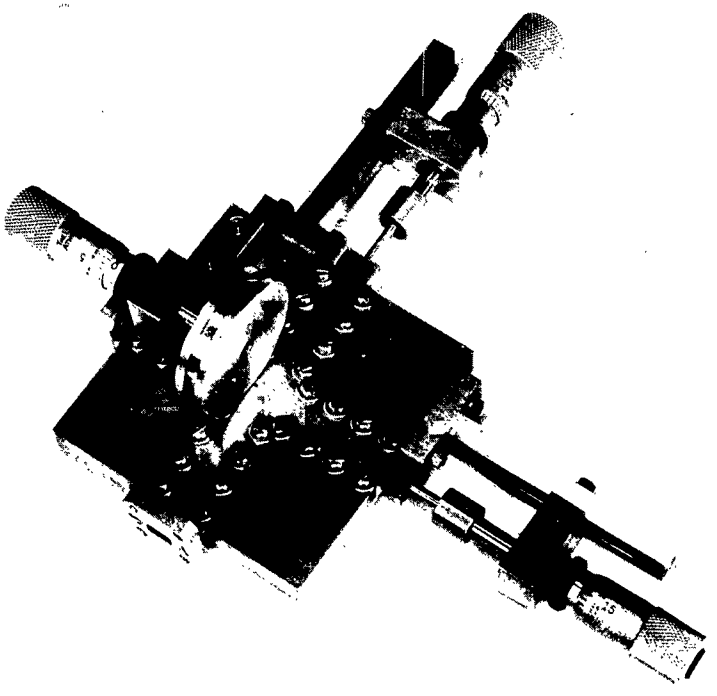

FIGURE 29. PHOTOGRAPH OF PHASE SHIFTER

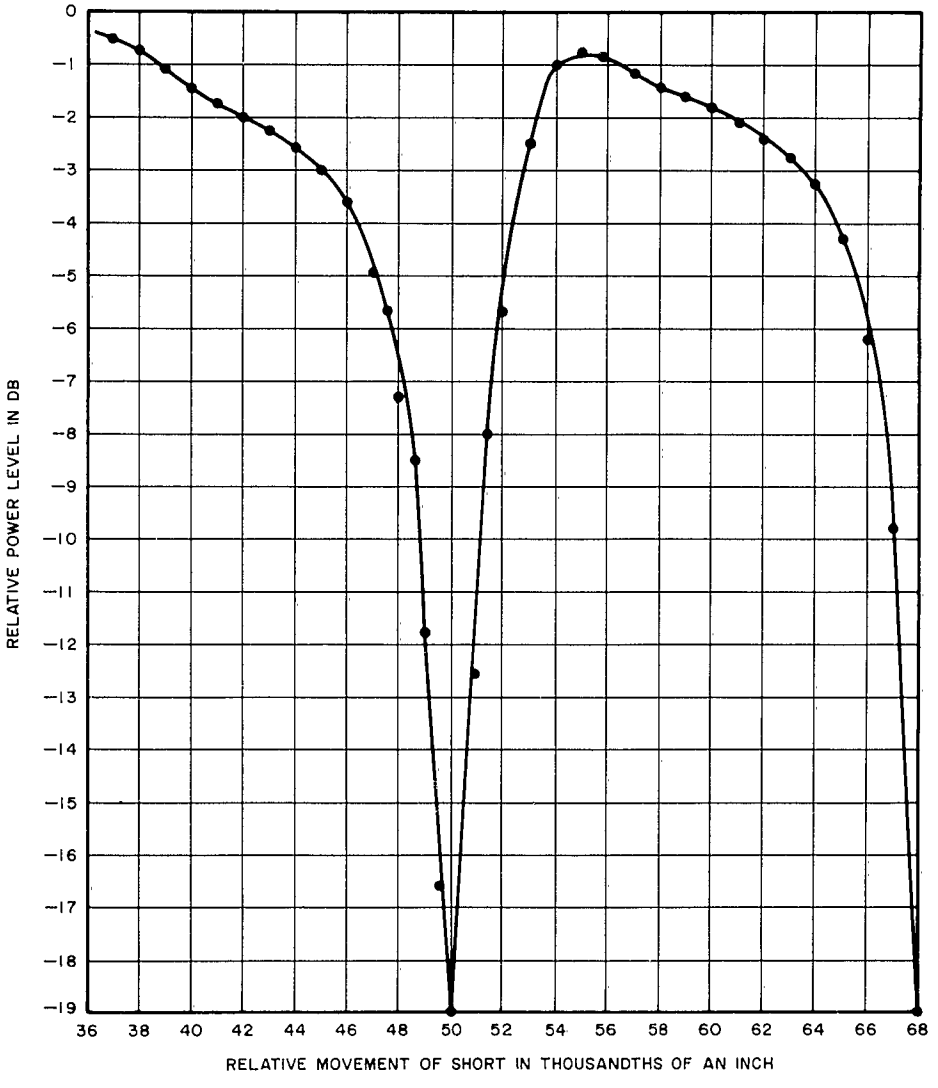

FIGURE 30. FRINGE PATTERN OBTAINED BY VARYING STRAIGHT-THROUGH-ARM SLIDING SHORT

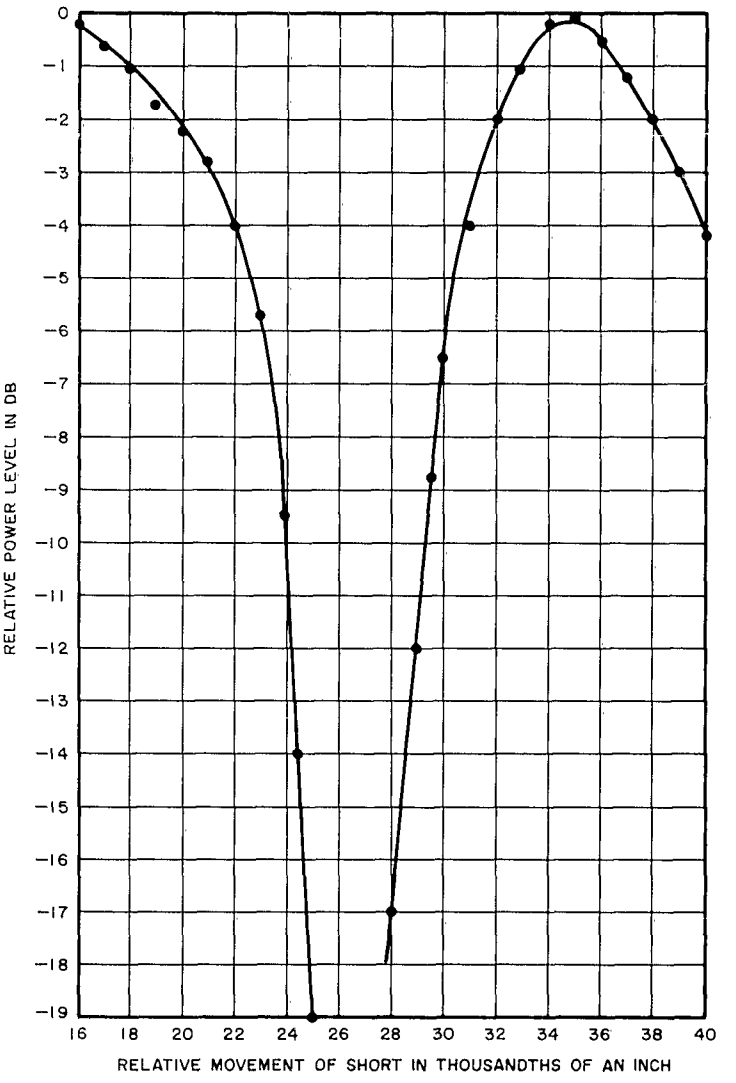

FIGURE 31. FRINGE PATTERN OBTAINED BY VARYING PERPENDICULAR-ARM SLIDING SHORT

IV. DESIGN CONSIDERATIONS

A. MATCHING

Proper impedance matching to eliminate air-dielectric interface reflections is of prime importance in all quasi-optical components. The power level in the decoupled port of the directional coupler is a function of the unwanted reflections in the other ports. The linearity of the phase shifter will be adversely affected by poor initial decoupling at the isolated port.

The air-dielectric interface reflections can be kept low by using a dielectric material with as low a relative dielectric constant as possible. For an air-dielectric interface, the reflection coefficient is:

$$|\Gamma| = \frac{\sqrt{\epsilon_r} - 1}{\sqrt{\epsilon_r} + 1}$$

From Figure 8 it can be seen that ϵ_r must be greater than 2 for a 45-degree incidence angle on the prism hypotenuse for total internal reflection to occur. This would correspond to $|\Gamma| = 0.167$ or an SWR of 1.4.

One of the more conventional means of eliminating reflections at the interface of two dielectric materials is to use quarter-wavelength matching transformers. To match a junction that uses materials that have ϵ_r's of ϵ_1 and ϵ_2, a material is inserted whose characteristic impedance is the geometric mean of the characteristic impedances in question. A material of $\epsilon_r = \epsilon_3$ where $\epsilon_3 = \sqrt{\epsilon_1 \epsilon_2}$ and whose electrical length is one-quarter wavelength at the frequency in question is used. The physical length of the matching section is $\ell = \lambda/4\sqrt{\epsilon_3}$. Theoretically, this device is a proper impedance transformer at only one frequency, but, in practice, it operates effectively over about a 10-percent bandwidth. This design theory can also be applied to give wider band matches by using many sections of dielectric material with appropriate lengths and dielectric constants.

Another technique for reducing reflection at the air-dielectric interface is to use appropriately sized slots

at the place of intersection (references 1 and 3). The value of ϵ required to produce a reflectionless quarter-wavelength transformer from air to dielectric is one of the solutions of

$$\zeta_1^2 - \zeta_1(\epsilon_r^{1/2} + 1) + \frac{\epsilon_r^{1/2}}{\epsilon_r^{1/2} + 1} = 0$$

and

$$\zeta_2^2 - \zeta_2\frac{(\epsilon_r^{1/2} + 1)}{\epsilon_r^{1/2}} + \frac{1}{\epsilon_r^{1/2} + 1} = 0$$

where

$$\zeta = \frac{a}{a + b},$$

a = width of slot,

$a + b$ = distance between centers of adjacent slots.

The solution is accurate for $a + b \leq 0.2\lambda$. The electrical depth of the slots is $\lambda/4$ or one-quarter wavelength.

For the prototype 27-Gc coupler, the matching problems were not severe. We made simple quarter-wavelength slabs of material with an ϵ_r of 1.6 (to match the Rexolite prisms).

In the construction of the Rexolite prism coupler for 0.9-mm operation, another problem was encountered. At 0.9 mm, one-quarter wavelength in an air medium is 0.0089 inch. Therefore, the physical length of the transformer was

$$\ell = \frac{0.0089}{1.6} = 0.0070 \text{ inch}$$

This calculation uses $\epsilon_r = 2.55$ for Rexolite. A slight error is incurred since $\epsilon_r = 2.45$ at 0.9 mm (Section VI-A). The size of the air bubbles in this material (foam) is greater than ℓ so that the surface of the slab presented to the incident radiation would be totally irregular. An alternative procedure is to use a slab many quarter-wavelengths thick, but this would decrease the bandwidth of the device considerably.

Slotting the dielectric is a satisfactory solution. For example, the solutions to the preceding equations are $\zeta_1 = 0.263$ and $\zeta_2 = 0.287$. Taking the intermediate value as the average of ζ_1 and ζ_2 gives $\zeta = a/(a + b) = 0.275$. In addition, the inequality $a + b \leq 0.2\lambda$ must be satisfied. For 0.9 mm, $\lambda = 0.040$ inch. The largest possible a + b dimension is assumed because the small size of a and b is the main problem--that is, a + b = 0.008 inch. Solving these two simultaneous equations gives a and b. We have developed a method for machining these small slots in Rexolite to close tolerances, and slotted Rexolite prisms for 0.9-mm operation have been successfully fabricated (Figure 12).

B. DIELECTRIC LOSSES AND DIELECTRIC CONSTANTS

Another important design consideration for the 0.9-mm quasi-optical oversize-waveguide components is the dielectric losses inherent in the materials. Information is lacking about the submillimeter range, not only with respect to the dielectric loss tangent (tan δ) but also for the value ϵ_r as a function of frequency. A literature search and a discussion with scientists at the Laboratory for Insulation Research at the Massachusetts Institute of Technology revealed that no data is available about dielectric properties in the submillimeter region. All available information is either in the microwave region up to 25 Gc (with some sparse data for 140 Gc) or at the end of the submillimeter region (far infrared). The data for the optical region of the spectrum is too far removed in frequency to be applicable. The highest frequency at which measurements of loss tangent have been made is 140 Gc (reference 16). However, the uncertainty factor at this frequency is two. An attempt was made to extend the theory of dielectric losses into the submillimeter region; however, the approximations for microwave and optical regions are not valid for the submillimeter region (references 17 and 18). The best that could be done was to extrapolate from available data in the initial design. This is also true for dielectric constants.

Unfortunately, many other dielectric materials have resonances in the loss-tangent-versus-frequency curve that occur in the submillimeter region at various unknown frequencies. They also have higher loss tangents at those frequencies for which data is available. Rexolite and quartz had the best probability of having low losses in the submillimeter region compared with other materials. Other physical properties such as availability, cost, weight, temperature-dependence of electrical characteristics, etc., indicate that Rexolite and quartz are the most feasible materials. Unfortunately, as the various insertion-loss data showed, these materials had high loss tangents.

C. COMPONENT FABRICATION

Tolerance problems were considered in these components because of possible mode conversion. Accurate machining of interior dimensions is important to minimize loss. The skin depth at 300 Gc is small and surfaces must be highly polished. The prism and multiple-slab coupling elements must present interfaces that appear smooth to $\lambda = 0.1$ cm. Typically, flatness to $\lambda/10$ or 0.01 cm was needed. The coupling devices must also be able to be moved in the waveguide without tilting. This has been achieved by careful mechanical design and construction. Difficulties were encountered with the movable shorts for the phase shifter because the concept of the usual choke type of short used in small waveguides was unsuitable optically; a plate type was needed. A highly polished noncontacting plate with a thin Teflon (0.002 inch) border was made to slide easily into the waveguide under the vernier micrometer drive. Little leakage was seen through the Teflon. A spring-finger contacting short would cause unknown higher-mode propagation effects and, in any case, good electrical contact is not critical for the quasi-optical oversize-waveguide type of transmission as far as the sliding shorts are concerned.

The final design for the devices was determined by all these considerations and good maching practice. No soldering was done on the components in order to facilitate the changing of interior coupler elements to experiment with matching, losses, etc. The fly-wheel and micrometer give extremely good control over the prism and slab movements.

D. POWER HANDLING

All of the components developed have power-handling requirements of at least 1 watt average and 1 kilowatt peak. The use of oversize-waveguide structures markedly increased the power-handling capacity over standard-size waveguide. The power flow in a TE_{10} mode rectangular waveguide is

$$P = \frac{ab\lambda E_m^2}{2\lambda g \eta}$$

where E_m is the rms magnitude of the electric field at the maximum point and η is the intrinsic impedance of free space. If a and b are both increased to 10 times their standard value, λ_g becomes approximately equal to λ and P becomes

$$P' = \frac{100\ abE_m^2}{2\lambda}$$

The increase in power handling for a given maximum electric field is therefore the ratio of P′ to P or 100 λ_g/λ. The improvement is at least 100 and, in many cases, as high as 150 (depending on λ_g/λ).

For the case of 0.140- by 0.280-inch waveguide used in our 0.9-mm components, we estimate that the theoretical breakdown power is at least 25 kilowatts. This estimate is based on the breakdown figures given in standard-waveguide tables for 9-mm waveguide. This estimate assumes that the critical field for breakdown at 0.9 mm is equal to that used in the 9-mm waveguide. This value is well above the 1-kilowatt level.

Dielectric structures are used in the components. Experience has shown that the peak power rating of dielectric materials is significantly lower than air. The exact figure varies from 10 to 20 percent depending on the material and its surface impurities. In any event, we can expect to handle 1 kilowatt because, even with the 10-percent factor, the peak power-handling capacity should be 2.5 kilowatts.

One final problem in satisfying the peak power-handling requirement is the avoidance of higher-mode resonances. If power is converted into higher modes that cannot be suitably damped, high Q resonances can occur that result in points of exceedingly high electric field. This problem is overcome because the components all have open ports that effectively terminate higher modes in a resistive load and prevent a high Q resonant-field build-up.

The average power requirement of 1 watt is easily met because the average power rating of 0.140- by 0.280-inch waveguide is 22 kilowatts.

Up to this point, we stressed operation in the vicinity of 0.9 mm. At 0.3 mm (the minimum wavelength under consideration), the power-handling capabilities would be 1/9 of those discussed if 10-times oversize waveguide is used. This would probably not be adequate from a peak-power standpoint. We could however use 30-times oversize waveguide in this case.

This discussion shows that estimates of the peak and average power handling satisfy the contract requirements. It is impossible to experimentally check the power-handling properties at this time because the best source of submillimeter power (the Lincoln Laboratory carcinotron) delivers only 10 milliwatts.

V. TESTS AND INSTRUMENTATION

A. POWER SOURCES

Two practical methods are presently available for generating useful power in the submillimeter region--crystal harmonic generators and carcinotron tubes, which produce 10 to 15 milliwatts at 330 Gc. It was determined that the price and delivery of the carcinotron and its associated power supply were beyond the scope of the contract. For this reason, work was started using a crystal harmonic generator. A Phillips DX-237 klystron was used as a fundamental source and Phillips or FXR crystal harmonic generators were used in attempts to triple from 110 to 330 Gc. The best result was 25 db of range in doubling from 115 to 230 Gc. We could not detect third-harmonic power through our squeeze-section filters even when we used homodyne or phase-lock receivers. The double-frequency power was also a sensitive function of harmonic-generator whisker pressure, time of use, etc., and appeared to be erratic in operation. We later gained access to the 330-Gc carcinotron and power supply at the Lincoln Laboratories. The carcinotron was more convenient for direct component testing and offered an improvement over harmonic-generator dynamic range. It was therefore decided to use the carcinotron, spend more time on the components and obtain more data.

B. TESTS

A block diagram of the test system used is shown in Figure 32. The carcinotron waveguide output is 4-times oversize at 330 Gc since standard waveguide has an attenuation of 10 db/foot at this frequency. We inserted a squeeze-section filter between our component and the 4-times oversize waveguide to ensure TE_{10} mode purity into our component. Initially, the power supply used was incapable of modulating the tube directly and a ferrite modulator using Faraday rotation was used before the bolometer detector. This detector was used because it was 10 db more sensitive than any available crystal detector. This modulation technique resulted in limitations in the dynamic range of our measurements. A modulating power supply was not available until nearly the end of the project. The frequency of the carcinotron was determined by either its frequency versus-anode-voltage calibration or our interferometer phase shifter. Agreement was within 2 Gc at a frequency of 328 Gc. Data-averaging techniques were used because drifts in the power supply could not be corrected.

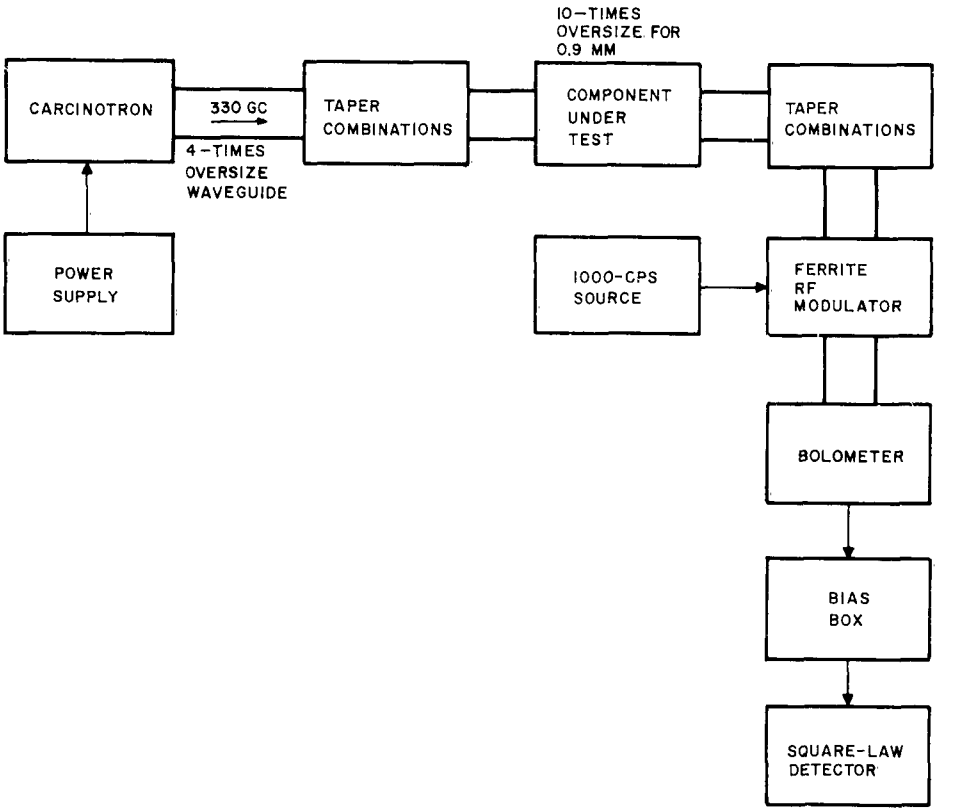

FIGURE 32. BLOCK DIAGRAM OF MEASUREMENT SETUP AT 0.9 mm

VI. ADDITIONAL MEASUREMENTS

A. MEASUREMENT OF DIELECTRIC CONSTANT

An additional result of the experiments with matched double-prism attenuators has been the accurate determination of the dielectric constant of Rexolite and quartz at 0.9 mm. The variation of attenuation (in db) with prism separation is

$$A = 10 \log \left[1 + \frac{(\epsilon_r - 1)^2}{\epsilon_r(\epsilon_r - 2)} \sinh^2 \alpha d \right]$$

where

$$\alpha = \frac{2\pi}{\lambda} \sqrt{\frac{\epsilon_r}{2} - 1}$$

which, for large αd ($\alpha d > 2$), becomes

$$A = 20 \log \left[\frac{\epsilon_r - 1}{2\sqrt{\epsilon_r(\epsilon_r - 2)}} \right] + 8.68\, \alpha d$$

The attenuation is a linear function of d for larger αd. The value of α can be obtained from measurements of the slope of the attenuation-versus-distance curve and, therefore, is a means of accurately obtaining ϵ_r.

By defining a slope m (equal to 8.68 α) we obtain

$$\epsilon_r = 2 \left[\left(\frac{m\lambda}{17.36\pi} \right)^2 + 1 \right]$$

The value of ϵ_r is therefore obtained directly from a measurement of the slope and the value of λ.

Using this technique on slot-matched Rexolite prisms and quarter-wavelength plate-matched quartz slabs with minimum ripple in the attenuation characteristic, we have been able to accurately determine the dielectric constants of Rexolite as $\epsilon_r = 2.45 \pm 0.01$ and of quartz as $\epsilon_r = 3.95 \pm 0.01$. These

values are somewhat less than the microwave-frequency values. The more points that are taken on the attenuation curve the more accurate is the determination of ϵ_r. The method is superior to that of the spectrometer, for example, in that the sensitivity is not a function of the material loss tangent.

B. MEASUREMENTS OF LOSS TANGENTS

As a part of the study, we measured the loss tangents (tan δ) of certain selected materials in the submillimeter region. We examined tan δ of Teflon, quartz, and Rexolite at 0.9 mm. The insertion loss of a given length of the material was measured at four frequencies around 0.9 mm (the range of the carcinotron). We used a sample in oversize waveguide with plane-wave propagation for which

$$\alpha = \frac{830\ \epsilon_r \tan \delta}{\lambda}$$

where α is the attenuation of a given sample length in db/foot and λ is the wavelength in cm. The values of α that we obtained were subject to certain small errors and therefore so is tan δ. For example, the materials are unmatched.

The results were:

Material	tan δ
Teflon	0.0004
Quartz	0.0043
Rexolite	0.0032

These numbers show total deterioration of the low-loss properties of quartz and Rexolite in the submillimeter region. However, they are consistent with our experimental results. Although Teflon is a low-loss material, it is not suitable for a 45-degree double-prism device due to its low dielectric constant (Figure 8). A materials study is necessary to determine low-loss materials in the 0.9-mm region.

VII. CONCLUSIONS

Several versions of four basic components operating in the submillimeter region have been designed, constructed, and tested. These components were a 0 to 40 db variable attenuator, a 10-db directional coupler, a greater than 90-degree variable phase shifter, and a 20-db transmitter-to-receiver isolation duplexer.

The advantages and disadvantages of various types of waveguide were evaluated. It has been seen that, though Goubau-beam waveguide has low losses as a transmission line, it is unsuitable for making small components and has the same problems as free-space techniques (interference from other RF circuits, influence of weather, lack of portability, etc.). Trough waveguide at submillimeter frequencies appears to have construction problems as a basic transmission line, and low-loss bends have not yet been devised. Submillimeter components using quasi-optical techniques were found to be convenient in size, low loss, and portable. The performance can be predicted theoretically and the components are shielded from environmental conditions. The use of this technique permits the components to be used in a practical system. The characteristics of these components (such as insertion loss, attenuation range, directivity, etc.) have been measured at submillimeter wavelengths within the limits set by the maximum power level (from the carcinotron) that the state of the art can produce. Such things as maximum power-handling ability and 40-db attenuation range could not be measured due to insufficient available power (typically, a 20-db dynamic range), but enough data has been taken to show the feasibility of using quasi-optical oversize-waveguide components.

These 4-port devices (each of which could be used as a variable attenuator, a variable directional coupler, or a duplexer) were made using the double-prism coupling element. The components were matched using slot matching or quarter-wavelength transformer techniques. These methods worked well. The main problem with these devices was the fact that the insertion loss of the dielectric prisms was high due to the poor qualities (loss tangent) of conventional low-loss-tangent materials (such as quartz and Rexolite) in the submillimeter region. The experimental data indicated that these materials had loss tangents of 0.0032 and 0.0047, respectively, at 0.9 mm. Before the advantages of the double-prism devices are to be fully realized, a study of material properties in

this region is necessary. The double-prism device has been used to measure the dielectric constants of quartz and Rexolite at 0.9 mm. These are $\epsilon_r = 3.95$ and 2.45, respectively. Also, the linear attenuation characteristics of the double-prism device together with the ability to accurately predict the magnitude of the attenuation with prism spacing makes these devices valuable as submillimeter attenuation standards. All of the components made are in waveguide and are easily used in systems.

A multiple-slab device has been constructed that has decreased the dielectric losses to about 2 db. This device uses matched quartz slabs and has been constructed and used as an attenuator or coupler. Its construction is more difficult than the double-prism devices, but it has been shown (theoretically and experimentally) to have lower loss.

The variable phase shifter provides variable phase shift over 360 degrees. It can be set to within about +2 degrees. It was used as an accurate interferometer (wavemeter) to determine the frequency of the carcinotron submillimeter source. Its operation is good except for the insertion loss due to the double-prism coupling element.

A grating duplexer was constructed without the inherent 6-db hybrid-duplexer loss. It operated with a transmitter receiver isolation of 28 db. The transmitter-receiver loss was 4 db. However, the gratings are frequency-sensitive and must be further studied to eliminate this dependence.

The basic double-prism or multiple-slab coupling structure in a 4-port device can be extended to develop other components for a complete submillimeter measurement system such as impedance transformers (E-H tuners), frequency meters, or standing-wave indicators. In addition, the quasi-optical oversize-waveguide technique is suitable for the development of filters, Faraday rotation devices, mixers, and varactor and detector mounts.

VIII. REFERENCES

1. R. H. Garnham, "Optical and Quasi-Optical Transmission Techniques and Component Systems for Millimeter Wavelengths," Royal Radar Establishment, Report 3020, March 1958.

2. L. Lewin, "A Note on Quasi-Optical Methods at Millimeter Wavelengths," Polytechnic Institute of Brooklyn, Microwave Research Institute Symposium on Millimeter Wave, p 469, 1959.

3. A. F. Harvey, "Optical Techniques at Microwave Frequencies," Proc IEE, Paper No. 2799E, p 154, March 1959.

4. H. G. Unger, "Circular Waveguide Taper of Improved Design," Bell System Technical Journal, Vol 37, p 899-912, July 1958.

5. J. Goldberg, et al., "Second Quarterly Progress Report on New Methods for Measuring Spurious Emissions," AIL Report No. 1112-I-2, Contract AF 30(602)-2511 for Rome Air Development Center, Deer Park, New York, November 1961.

6. H. J. Hindin and J. J. Taub, "An Oversize Waveguide Directional Coupler," IRE Transactions on Microwave Theory and Techniques, Vol MTT-10, p 394, September 1962.

7. M. Cohn, "Propagation in a Dielectric-Loaded Parallel Plane Waveguide," IRE Transactions on Microwave Theory and Techniques, Vol MTT-7, p 202-208, April 1959.

8. M. Cohn, "TE Modes of the Dielectric Loaded Trough Line," IRE Transactions on Microwave Theory and Techniques, Vol MTT-8, p 449-454, July 1960.

9. M. Cohn, F. Sobel, and J. M. Cotton, "Millimeter Wave Research," Technical Note No. 1, Contract AF 30(602)-2457, Rome Air Development Center, November 1961.

10. J. M. Cotton, et al., "Millimeter Wave Research," Final Technical Report, Contract AF 30(602)-2457, Electronic Communications, Inc., December 1962.

11. G. Goubau and F. Schwering, "On the Guided Propagation of Electromagnetic Wave Beam," IRE Transactions on Applied Physics, Vol AP-9(3), p 248-256, May 1961.

12. J. R. Christian and G. Goubau, "Experimental Studies on a Beam Waveguide for Millimeter Waves," IRE Transaction on Applied Physics, Vol AP-9(3), p 256-263, May 1961.

13. C. Schaefer and G. Gross, "Investigations Concerning Total Reflection," Annalen Der Physik, Vol 32, p 648, 1910.

14. R. G. Fellers, "Applications of Dielectric Prisms at Millimeter Wavelengths," University of South Carolina, Department of Electrical Engineering, ASTIA Document No. AD-219785, July 1959.

15. R. G. Fellers, "A Circular Polarization Duplexer for Millimeter Waves," Trans AIEE, p 934-937, January 1960.

16. M. J. King, et al., "Quasi-Optical Components and Surface Waveguides for the 100 to 300 kMc Frequency Range," Electronic Communications, Inc., Contract AF 19(604)-5475, November 1960.

17. A. R. Von Hippel, "Dielectrics and Waves," John Wiley & Sons, Inc., New York, 1954.

18. A. R. Von Hippel, "Dielectric Materials and Applications," Technology Press of the Massachusetts Institute of Technology, Boston, 1954.

19. L. Storch, "The Transmission Matrix of N Alike Cascaded Networks," AIEE Transactions, Vol 73, Part 1, p 616-618, January 1955.

APPENDIX I

REFLECTION AND TRANSMISSION PROPERTIES OF A PAIR OF MOVABLE DIELECTRIC SLABS

The movable dielectric slabs of Figure 22A have relative dielectric constants ϵ_r, are assumed to be lossless, and have a thickness t equal to 90 electrical degrees. The object of this analysis is to obtain the reflection and transmission coefficients as functions of the slab separation d_1. The impedance at plane b for a 90-degree dielectric slab is

$$Z_b = \frac{Z_\epsilon^2}{Z_a} \qquad \text{(I-1)}$$

where

$Z_a = 120\pi\sqrt{2}$ = characteristic impedance in air for a direction 45 degrees from the vertical,

Z_ϵ = characteristic impedance in the dielectric for a wave that is traveling in a direction of 45 degrees at the air interface.

$$Z_\epsilon = \frac{120\pi}{\sqrt{\epsilon_r}} \sec \theta_2$$

where $\sin \theta_2 = \frac{\sin 45}{\sqrt{\epsilon_r}}$. Then,

$$Z_\epsilon = 120\pi \sqrt{\frac{2}{2\epsilon_r - 1}}$$

The impedance at plane c as obtained from transmission-line theory is

$$Z_c = Z_\epsilon \left[\frac{Z_b + jZ_a \tan \frac{2\pi d_1}{\sqrt{2}\lambda}}{Z_a + jZ_b \tan \frac{2\pi d_1}{\sqrt{2}\lambda}} \right] \qquad \text{(I-2)}$$

From which,

$$Z_d = \frac{Z_\epsilon^2}{Z_c} = \frac{120\pi\sqrt{2}\left[Z_a + jZ_b \tan \frac{2\pi d_1}{\sqrt{2}\lambda} \right]}{(2\epsilon_r - 1)\left[Z_b + jZ_a \tan \frac{2\pi d_1}{\sqrt{2}\lambda} \right]} \qquad \text{(I-3)}$$

From equation I-3, the reflection coefficient at plane d is

$$\Gamma_d = \frac{Z_d - Z_a}{Z_d + Z_a} = \frac{j \tan \frac{2\pi d_1}{\sqrt{2}\lambda} \left[\frac{1}{(2\epsilon_r - 1)^2} - 1 \right]}{j \tan \frac{2\pi d_1}{\sqrt{2}\lambda} \left[\frac{1}{(2\epsilon_r - 1)^2} + 1 \right] + \frac{2}{2\epsilon_r - 1}} \qquad \text{(I-4)}$$

The power (P_2) coupled to port 2 is $|\Gamma_d|^2 P_1$. From equation I-4, $|\Gamma_d|^2$ is:

$$\frac{P_2}{P_1} = |\Gamma_d|^2 = \frac{\tan^2(0.707\theta_1)\left[\left(\frac{1}{2\epsilon_r - 1} \right)^2 - 1 \right]^2}{\left(\frac{2}{2\epsilon_r - 1} \right)^2 + \tan^2(0.707\theta_1)\left[\left(\frac{1}{2\epsilon_r - 1} \right)^2 + 1 \right]^2} \qquad \text{(I-5)}$$

where $\theta_1 = \frac{2\pi d_1}{\lambda}$.

For lossless slabs, the power (P_3) coupled to port 3 is $(1 - |\Gamma_d|^2)\, P_1$. Therefore,

$$\frac{P_3}{P_1} = 1 - |\Gamma_d|^2 = \frac{\left(\frac{2}{2\epsilon_r - 1}\right)^2 \sec^2(0.707\theta_1)}{\left(\frac{2}{2\epsilon_r - 1}\right)^2 + \tan^2(0.707\theta_1)\left[\left(\frac{1}{2\epsilon_r - 1}\right)^2 + 1\right]^2} \tag{I-6}$$

APPENDIX II

REFLECTION AND TRANSMISSION PROPERTIES OF A PAIR OF MOVABLE DOUBLE SLABS

The reflection and transmission coefficients of the double-slab structure shown in Figure 22B (slabs 3 through n are not considered) will be derived. The impedance at plane d is obtained from equation I-3. In this structure, $\frac{2\pi d_1}{\sqrt{2}\lambda}$ is chosen to be $\frac{\pi}{2}$. Thus,

$$Z_d = \frac{120\pi\ Z_b\ \sqrt{2}}{(2\epsilon_r - 1)\ Z_a} = \frac{120\pi\ \sqrt{2}}{(2\epsilon_r - 1)^2} \qquad \text{(II-1)}$$

The impedance at plane e is

$$Z_e = Z_a \left[\frac{Z_d + jZ_a \tan \frac{2\pi d_2}{\sqrt{2}\lambda}}{Z_a + jZ_d \tan \frac{2\pi d_2}{\sqrt{2}\lambda}} \right] \qquad \text{(II-2)}$$

Transforming Z_e through a quarter-wavelength section of Z_ϵ, we obtain,

$$Z_f = \frac{Z_\epsilon^2}{Z_e} \qquad \text{(II-3)}$$

Similarly,

$$Z_g = \frac{Z_\epsilon^2}{Z_f} \qquad \text{and} \qquad Z_h = \frac{Z_\epsilon^2}{Z_g} \tag{II-4}$$

Using equations II-2, II-3, and II-4:

$$Z_h = Z_a \left(\frac{Z_g}{Z_a}\right)^4 \left[\frac{1 + j \frac{Z_d}{Z_a} \tan \frac{2\pi d_2}{\sqrt{2}\lambda}}{\frac{Z_d}{Z_a} + j \tan \frac{2\pi d_2}{\sqrt{2}\lambda}}\right] \tag{II-5}$$

which reduces to

$$Z_h = 120\pi \sqrt{2} \left(\frac{1}{2\epsilon_r - 1}\right)^2 \left[\frac{1 + j \left(\frac{1}{2\epsilon_r - 1}\right)^2 \tan \frac{2\pi d_2}{\sqrt{2}\lambda}}{\left(\frac{1}{2\epsilon_r - 1}\right)^2 + j \tan \frac{2\pi d_2}{\sqrt{2}\lambda}}\right] \tag{II-6}$$

The reflection coefficient at plane h is

(II-7)

$$\Gamma_h = \frac{Z_h - Z_a}{Z_h + Z_a} = \frac{j \tan \frac{2\pi d_2}{\sqrt{2}\lambda} \left[\left(\frac{1}{2\epsilon_r - 1}\right)^4 - 1\right]}{2\left(\frac{1}{2\epsilon_r - 1}\right)^2 + j \tan \frac{2\pi d_2}{\sqrt{2}\lambda} \left[\left(\frac{1}{2\epsilon_r - 1}\right)^4 + 1\right]}$$

Finally, the power reflection coefficient $|\Gamma_h|^2$ is

$$\frac{P_2}{P_1} = |\Gamma_h|^2 = \frac{\tan^2(0.707\theta_2)\left[\left(\frac{1}{2\epsilon_r - 1}\right)^4 - 1\right]^2}{4\left(\frac{1}{2\epsilon_r - 1}\right)^4 + \tan^2(0.707\theta_2)\left[\left(\frac{1}{2\epsilon_r - 1}\right)^4 + 1\right]^2} \qquad \text{(II-8)}$$

where $\theta_2 = \frac{2\pi d_2}{\lambda}$ and the power transmission coefficient $1 - |\Gamma_h|^2$ is

$$\frac{P_3}{P_1} = 1 - |\Gamma_1|^2 = \frac{4\left(\frac{1}{2\epsilon_r - 1}\right)^4 \sec^2(0.707\theta_2)}{4\left(\frac{1}{2\epsilon_r - 1}\right)^4 + \tan^2(0.707\theta_2)\left[\left(\frac{1}{2\epsilon_r - 1}\right)^4 + 1\right]^2} \qquad \text{(II-9)}$$

APPENDIX III

DISSIPATION IN MULTIPLE-SLAB COUPLERS

Appendixes I and II show that 100-percent transmission of the incident power to port 3 occurs when the separation, d_2, of one set of slabs to the other is 0.707λ assuming lossless dielectrics. The effect of loss in the dielectric slabs reduces the power delivered to port 3. The purpose of this appendix is to compute this loss for a coupler having n slabs with each slab characterized by the same dielectric constant and loss tangent. The analysis is based on obtaining the ABCD matrix for ports 1 and 3. The insertion loss is then obtained from (reference 19)

$$L = 10 \log \frac{|A + B + C + D|^2}{4} \qquad \text{(III-1)}$$

The overall ABCD matrix is obtained by determining the matrices of the individual slab elements and then multiplying them. The ABCD matrix of a quarter-wavelength dielectric slab (for small dissipation; that is, $\alpha t < 0.1$) is given by

$$\begin{pmatrix} j\alpha t & j(2\epsilon_r - 1)^{-1/2} \\ j(2\epsilon_r - 1)^{1/2} & j\alpha t \end{pmatrix} \qquad \text{(III-2)}$$

where

$$\alpha t = \frac{\pi \epsilon_r \tan \delta}{2(2\epsilon_r - 1)}$$

for t corresponding to a quarter-wavelength condition.

The matrix for a quarter-wavelength section of air is

$$\begin{pmatrix} 0 & j \\ j & 0 \end{pmatrix} \qquad \text{(III-3)}$$

We can now define a typical dielectric-air section by the matrix (M) as

$$(M) = \begin{pmatrix} j\alpha t & j(2\epsilon_r - 1)^{-1/2} \\ j(2\epsilon_r - 1)^{1/2} & j\alpha t \end{pmatrix} \begin{pmatrix} 0 & j \\ j & 0 \end{pmatrix}$$

$$= \begin{pmatrix} -k & -\alpha t \\ -\alpha t & -1/k \end{pmatrix} \qquad \text{(III-4)}$$

where $k = (2\epsilon_r - 1)^{-1/2}$

A wave propagating from ports 1 to 3 must traverse n dielectric-air sections, a single section of air equivalent to a quarter wavelength ($d_2/2$, when d_2 is set at 0.707λ), and another set of n dielectric-air sections. This is expressed as

$$\begin{pmatrix} A & B \\ C & D \end{pmatrix} = (M)^n \begin{pmatrix} 0 & j \\ j & 0 \end{pmatrix} (M)^n \qquad \text{(III-5)}$$

With the aid of reference 19, this can be expanded for any n as follows

$$\begin{pmatrix} A & B \\ C & D \end{pmatrix}^n = \begin{pmatrix} P_nA - P_{n-1} & P_nB \\ P_nC & -P_nD \end{pmatrix} \qquad \text{(III-6)}$$

P_n is defined by the recursion formula

$$P_n = (A + D)\, P_{n-1} - P_{n-2} \qquad \text{(III-7)}$$

where

$$P_0 = 0,$$
$$P_1 = 1,$$
$$P_2 = A + D = -\left(k + \frac{1}{k}\right).$$

Substituting equation III-6 into III-5 and performing the indicated matrix multiplication yields

$$\begin{pmatrix} A & B \\ C & D \end{pmatrix} = \begin{pmatrix} j2\alpha t P_n\left(kP_n + P_{n-1}\right) & j\left(\frac{P_n}{k} + P_{n-1}\right)\left(kP_n + P_{n-1}\right) \\ j\left(P_n k + P_{n-1}\right)\left(\frac{P_n}{k} + P_{n-1}\right) & j2\alpha t P_n\left(\frac{P_n}{k} + P_{n-1}\right) \end{pmatrix} \qquad \text{(III-8)}$$

From equations III-8 and III-1, the insertion loss is

$$L = 10 \log \frac{\left|4\alpha t P_n P_{n-1} + 2\alpha t P_n^2\left(k + \frac{1}{k}\right) + 2P_n^2 + 2P_{n-1}^2 + 2P_n P_{n-1}\left(k + \frac{1}{k}\right)\right|^2}{4} \qquad \text{(III-9)}$$

Using the recursion formula (equation III-7) for P_n, we can express equation III-9 for specific cases of n = 1, 2, and 3 as follows.

For n = 1,

$$L = 10 \log \left[1 + \pi\epsilon_r \tan\delta\, k^2\left(k + \frac{1}{k}\right)\right] \qquad \text{(III-10)}$$

For n = 2,

$$L = 10 \log \left\{ 1 + \pi \epsilon_r \tan \delta \, k^2 \left[\left(k + \frac{1}{k} \right)^3 - 2 \left(k + \frac{1}{k} \right) \right] \right\} \qquad \text{(III-11)}$$

For n = 3,

$$L = 10 \log \left\{ 1 + \pi \epsilon_r \tan \delta \, k^2 \left[\left(k + \frac{1}{k} \right)^2 - 1 \right] \left(k + \frac{1}{k} \right) \left[\left(k + \frac{1}{k} \right)^2 - 3 \right] \right\} \qquad \text{(III-12)}$$

APPENDIX IV

CIRCULAR-POLARIZATION DISTORTION BY RECTANGULAR WAVEGUIDE

The purpose of this appendix is to determine the effect of propagating a circularly polarized wave in rectangular oversize waveguide. In order to do this, we will determine the maximum allowable length of rectangular waveguide between the circular-polarization grating and the target port.

Circular-polarization distortion arises because the two orthogonal waves have slightly different phase velocities. The waveguide wavelengths for the electric-field components parallel and perpendicular to the broad dimensions of the waveguide are:

$$\lambda_{gH} = \frac{\lambda}{\sqrt{1 - \left(\frac{\lambda}{2a}\right)^2}} \quad \text{and} \quad \lambda_{gV} = \frac{\lambda}{\sqrt{1 - \left(\frac{\lambda}{2b}\right)^2}} \qquad \text{(IV-1)}$$

The differential phase shift for a length equal to λ is:

$$\phi_H - \phi_V = 2\pi\lambda \left(\frac{1}{\lambda_{gH}} - \frac{1}{\lambda_{gV}}\right) \frac{\text{radians}}{\text{wavelength}} \qquad \text{(IV-2)}$$

Substituting equation IV-1 into equation IV-2

$$\phi_H - \phi_V = 180 \left[\left(\frac{\lambda}{2b}\right)^2 - \left(\frac{\lambda}{2a}\right)^2\right] \frac{\text{degrees}}{\text{wavelength}} \qquad \text{(IV-3)}$$

since $\left(\frac{\lambda}{2a}\right)^2 << 1$ and $\left(\frac{\lambda}{2b}\right)^2 << 1$ for oversize waveguide.

For the oversize waveguide used in the circular-polarization duplexer, a = 0.280 inch and b = 0.140 inch. The wavelength is 0.036 inch. Substituting these values in equation IV-3 gives

$$\phi_H - \phi_V = 2.23 \text{ degrees/wavelength}$$

This calculation shows that the length of oversize waveguide should be short--less than two wavelengths for example. To minimize any distortion caused by this effect in the experimental work on the duplexer, the target was butted against grating B.

DISTRIBUTION LIST FOR REPORT NO. 2098-1

Copy No.	Address		No. of Copies
1&2	**RADC (RALTM, ATTN: Mr. LoMascolo) Griffiss AFB, New York		2
3	*RADC (RAAPT) Griffiss AFB, New York		1
4	*RADC (RAALD) Griffiss AFB, New York		1
5	*GEEIA (ROZMCAT) Griffiss AFB, New York		1
6	*RADC (RAIS, ATTN: Mr. Malloy) Griffiss AFB, New York		1
7	*US Army Electronics R&D Labs Liaison Officer RADC Griffiss AFB, New York		1
8	*AUL (3T) Maxwell AFB, Ala		1
9	ASD (ASAPRD) Wright-Patterson AFB, Ohio		1
10	Chief, Naval Research Lab ATTN: Code 2027 Washington 25, D.C.		1
11	Commanding Officer US Army Electronics R&D Labs ATTN: SELRA/SL-ADT Ft. Monmouth, New Jersey		1
12	AFSC (SCSE) Andrews AFB Washington 25, D.C.		1
13-22	*ASTIA (TISIA-2) Arlington Hall Station Arlington 12, Va.	(If not releasable to ASTIA, IAW AFR 205-43, send the 10 copies to RADC (RAAPP-2) for secondary distribution)	Minimum of 10 copies

DISTRIBUTION LIST FOR REPORT NO. 2098-1 (cont)

Copy No.	Address	No. of Copies
23	Electronic Communications, Inc. ATTN: Dr. J. Wiltse 1830 York Road Timonium, Md.	1
24	RADC (RAWED/Mr. R. Davis) Griffiss AFB, New York	1
25	Commanding Officer USAERDL ATTN: SELRA/SL-PEE/Mr. N. Lipetz Ft. Monmouth, New Jersey	1
26	Bureau of Ships Electronic Division ATTN: Mr. L. V. Gumina Washington 25, D.C.	1
27	Sylvania Electronic Systems ATTN: Mr. R. Johnson 1100 Wherle Drive Buffalo 21, New York	1
28	University of Illinois ATTN: Dr. P. V. Coleman College of Engineering Urbana, Illinois	1
29	Raytheon Company ATTN: Mr. F. McVoy 6380 Hollister Avenue Santa Barbara, California	1
30	Polytechnic Institute of Brooklyn ATTN: Dr. A. A. Oliner Microwave Research Institute 55 Johnson Street Brooklyn, New York	1
31	FXR ATTN: Mr. L. Bertan 26-12 Borough Place Woodside 77, New York	1
32	Sperry Microwave Co. ATTN: Mr. R. Duncan Clearwater, Florida	1
33	Microwave Associates ATTN: Dr. L. Gould Burlington, Massachusetts	1

DISTRIBUTION LIST FOR REPORT NO. 2098-1 (cont)

Copy No.	Address	No. of Copies
34	University of Wisconsin ATTN: Dr. Scheibe Dept. of Electrical Engineering Madison, Wisconsin	1
35	AFCRL ATTN: Mr. F. J. Zucker Electromagnetic Radiation Lab Bedford, Massachusetts	1
36	NASA ATTN: Dr. Robert Coates, Code 520.1 Goddard Space Flight Center Greenbelt, Maryland	1
37	Director Ballistic Research Lab Aberdeen Proving Ground Aberdeen, Maryland	1
38	Aerospace Corp. ATTN: Dr. R. C. Hansen Electronics Lab PO Box 95085 Los Angeles 25, California	1
39	MIT Lincoln Laboratory ATTN: Mr. G. Catuna Lexington 73, Massachusetts	1
40	The Martin Co. ATTN: Dr. Vernon C. Derr Orlando, Florida	1
41	Lawrence Radiation Laboratory ATTN: Mr. Charles B. Whanton University of California PO Box 808 Livermore, California	1
42&43	Advisory Group on Electronic Devices ATTN: Mr. W. Kramer 346 Broadway, 8th Floor New York 13, New York	2
44	Boulder Laboratory ATTN: Dr. J. M. Richardson National Bureau of Standards Boulder, Colorado	1

DISTRIBUTION LIST FOR REPORT NO. 2098-1 (cont)

Copy No.	Address	No. of Copies
45	USASRDL ATTN: Mr. Leonard Hatkin Chief, Antenna & Microwave Circuitry Section Belmar, New Jersey	1
46	The Johns Hopkins University Department of Electrical Engineering ATTN: Dr. Harvey Palmer Baltimore 18, Maryland	1
47	Massachusetts Institute of Technology ATTN: Dr. Alan H. Barrett Room 26-459 Cambridge, Massachusetts	1
48	USAERDL ATTN: Dr. George Goubau Ft. Monmouth, New Jersey	1
49	Columbia University ATTN: Dr. S. P. Schlesinger Department of Electrical Engineering New York 27, New York	1
50	University of Illinois ATTN: Professor Paul E. Mayes Department of Electrical Engineering 212 Electrical Engineering Research Laboratory Urbana, Illinois	1

** Project Engineer will enter his office symbol and name in space provided.

* Mandatory.